Theor Chem Acc (1999) 103:87–104
DOI 10.1007/s002149900007

Theoretical
Chemistry Accounts

Regular article

Monte Carlo algorithms for simulating systems with adiabatic separation of electronic and nuclear degrees of freedom

Bin Chen, J. Ilja Siepmann

Department of Chemistry, University of Minnesota, 207 Pleasant Street SE, Minneapolis, MN 55455-0431, USA

Received: 22 December 1998 / Accepted: 5 January 1999 / Published online: 21 June 1999

Abstract. Two Monte Carlo algorithms for the adiabatic sampling of nuclear and electronic degrees of freedom are introduced. In these algorithms the electronic degrees of freedom are subject to a secondary low-temperature thermostat in close analogy to the extended Lagrangian formalism used in molecular dynamics simulations. Numerical tests are carried out for two model systems of coupled harmonic oscillators, and for two more realistic systems: the water dimer and bulk liquid water. A statistical-mechanical discussion of the partition function for systems with adiabatic separation of electronic and nuclear degrees of freedom, but with finite electronic temperature, is presented. The theoretical analysis shows that the algorithms satisfy the adiabatic limit using suitable choices of the electronic temperature, T_{elec}, the number of electronic moves, R_{elec}, and the maximum step sizes used for displacements of nuclear coordinates. For quadratic coupling of the nuclear and electronic degrees of freedom, the electronic phase-space volume is independent of the nuclear coordinates. In this case, the sampling of the nuclear coordinate phase-space recovers the correct Born-Oppenheimer limit independent of T_{elec}, but each electronic degree of freedom contributes an offset of $0.5k_{\mathrm{B}}T'_{\mathrm{elec}}$ (with $T'^{-1}_{\mathrm{elec}} = T^{-1} + T^{-1}_{\mathrm{elec}}$) to the average total energy. For nonquadratic coupling, satisfactory sampling of the nuclear coordinate phase-space requires a low T_{elec} to limit the ratio of the electronic phase-space volumes at T_{elec} and T'_{elec} to be close to unity.

Key words: Monte Carlo algorithms – Adiabatic sampling – Polarizable force fields

1 Introduction

Over the last two decades, our microscopic-level understanding of the thermodynamic behavior of complex molecular systems has been advanced by large-scale computer simulations. Such simulations are in principle able to provide an exact connection between a given microscopic model and its macroscopic properties. However, the major approximation in computer simulations is the force field used to describe the model system, which affects the accuracy of the prediction. Force fields reflect our limited knowledge of molecular interactions and our finite computational resources. The force fields used in computer simulations describe molecules as sets of connected interaction sites and decompose the complex electrostatic interactions into individual components, for example, Coulombic potentials for charge-charge interactions and Lennard–Jones potentials for electron repulsion and dispersion interactions. Therefore, the validity of force fields should not be determined solely by how accurate they can reproduce selected experimental results, but also by their quantum-mechanical basis. It is obvious that a more complex force field should yield better predictions of experimental data and should be closer to the physical reality. Unfortunately, in practice, a compromise has to be found between the complexity of the force field, the ability to determine all force field parameters, and the finite computational resources. Thus a good force field will represent such a compromise at a given time, but will undergo changes as more experimental results become available, as computer power increases, and as novel sampling algorithms are developed. One illustrative example is the modeling of the electronic structure of molecules. Most common force fields use fixed partial charges on defined sites in the molecular frame. In such an effective pairwise additive force field, many-body effects are approximated in a mean-field way, and the force field works best for the particular thermodynamic state for which it has been derived. Consequently, this restricts the transferability of such a force field to other thermodynamic states. Problems are more severe for highly charged and polarizable systems, where the charge conformation on a given molecule is strongly affected by its surroundings. Such situations will require the explicit incorporation of many-body effects. Due to limitations in computational resources and simulation

Correspondence to: J.I. Siepmann
e-mail: siepmann@chem.umn.edu

techniques, effective pair potentials have dominated for a long time [1, 2], even for highly polarizable systems, such as water. In particular for water, however, there is an upsurgance of many polarizable force fields [3–9].

The most important innovation for molecular dynamics simulations of polarizable models is the Car–Parrinello method [10], based on an extended Lagrangian formalism [3, 10–13]. The other established method is based on an iterative procedure to achieve the adiabatic separation required by polarizable models and to minimize the electronic energy at every change of configuration [7, 14–16]. It has been pointed out that the iterative scheme has to be carried out to a very high degree of convergence in order to conserve energy for the nuclear dynamics, or there will be a systematic drag force and the electronic system will behave like a heat sink [2, 17]. The Car–Parrinello method [10] elegantly broadened the scope of systems that could be studied. In this approach, the electronic density (described via density functional theory expanded in a plane-wave basis set) is treated as additional dynamical variables and an extended Lagrangian formalism is used to solve the equations of motion, where the adiabatic limit is maintained by an "on-the-fly" optimization using small masses for the electronic degrees of freedom. The electronic forces fluctuate around their adiabatic values, i.e. the electronic configuration is not exactly in its ground state; however, the fluctuations are random and can be made small by maintaining a sufficiently low temperature for the electronic motion [18]. The instantaneous forces due to the electronic configuration do not coincide with the instantaneous Born–Oppenheimer (BO) surface, but time averages of both agree to high accuracy [19, 20]. The electronic motions behave as fast oscillators [19], and the low electronic temperature results in a finite skin thickness of the BO surface [10]. When the nuclei move in-between the fast oscillators, the Hamiltonian of a system containing both fast and slow variables can be approximated by an "averaged" Hamiltonian obtained by performing an average over the fast coordinates [19]. In this respect, increasing the temperature or the masses for the electronic degrees of freedom allows one to use a larger time increment for the nuclear degrees of freedom. Unfortunately, as pointed out by Car and Parrinello [10], the resulting large thickness of the BO surface will not only cause the forces to be wrongly estimated, but also cause them to be dependent on the path along which a given point on the potential energy surface is approached. Most molecular dynamics simulations for polarizable force fields have used an electronic temperature of 5 K [6, 18].

As the Car–Parrinello method has opened new areas for molecular dynamics simulations, the methodology development in the Monte Carlo (MC) area has been lagging behind. One reason that makes it difficult to transplant the Car–Parrinello concept into a MC algorithm stems from the orthonormality constraints put on the wave functions. As pointed out by Relmer and Madden [17], in MC simulations the trial move must be random, but to achieve this randomness in the presence of constraints is not straightforward; thus, the only technique available for MC simulations of polarizable models has been the iterative scheme [7, 14–16]. Similar to the molecular dynamics case, very high accuracy of the iterative scheme is also required in MC simulations to yield the correct acceptance probabilities and to satisfy the detailed balance condition. In addition, the fact that the electronic structure should be optimized at every move (i.e. N times per cycle) makes this method extremely computer intensive and compares very unfavorably to molecular dynamics where iterations are required only once every time step. A small increase of only 10% in the computing time has been reported for molecular dynamics simulations using the extended Lagrangian formalism for polarizable water models compared to the corresponding fixed-charge models [6]. In contrast, for MC simulations of polarizable models an increase of 2 orders of magnitude has been observed using an iterative scheme for relatively small systems [14]. Nevertheless, for many optimization problems (other than the electronic-structure problem) the MC method is as efficient as molecular dynamics for performing simulated annealing. Thus, in principle, the MC method should be a viable alternative for some model systems, in particular for those in which there are no constraints or the constraints can be easily satisfied. It should be pointed out that such a MC scheme for polarizable force fields will allow for simulations in the grand-canonical and Gibbs ensemble that are not easily amenable to molecular dynamics techniques.

In a previous communication [21] we introduced a novel MC algorithm for polarizable force fields (with the simple constraint of molecular neutrality, i.e. no charge transfer between molecules) which attempts to mimic the Car–Parrinello approach in the context of the MC framework. Many questions remained unanswered in Ref. [21]. The most obvious question concerning the results is that, by applying the MC algorithm to the simple point charge-fluctuating charge (SPC-FQ) water model [6], the energies and the structures obtained did not agree with those calculated by Rick et al. [6] using molecular dynamics techniques. One reason suggested in Ref. [21] was that the differences may be caused by the different treatments of the long-range electrostatic interactions (Ewald summation was used in the molecular dynamics simulations, while a group-based potential truncation was used in the MC simulations). Regarding the technical aspects, Ref. [21] did not elaborate on the partition function of this polarizable system. There are two different temperatures for two different types of degrees of freedom. Are these two temperatures involved in the partition function or can the faster (or electronic) one be averaged out? Another unsolved question is whether sequential random moves of the electronic and nuclear degrees of freedom can be used in MC simulations, which contradicts the physical fact that during every nuclear move there is a simultaneous update of the electronic configuration. This may imply a possible danger: favoring of the initial state over the trial state for every nuclear move. More interestingly, how can MC simulations realize the adiabatic separation of the nuclear and electronic motion without employing large differences in nuclear and electronic masses as required in the molecular dynamics technique?

The purpose of this work is to answer the questions posed above, to introduce a modified MC algorithm for the adiabatic sampling of electronic and nuclear degrees of freedom, and to show the applicabilities and validities of these MC algorithms from numerical tests and theoretical arguments. The remainder of this article is arranged as follows. A detailed description of the MC techniques used in this work is given in Sect. 2. In Sect. 3 numerical tests of these algorithms on two model problems consisting of coupled harmonic oscillators are presented. In Sects. 4 and 5, canonical-ensemble simulations of the confined water dimer and bulk liquid water are described. Ways to improve the efficiency of the MC algorithms are discussed in Sect. 6. Section 7 provides a statistical-mechanical analysis of the canonical partition function for polarizable models. Conclusions and future extensions are outlined in Sect. 8.

2 Simulation methods

Since much of our discussion about MC algorithms for sampling electronic and nuclear degrees of freedom will focus on the SPC-FQ water model developed by Rick et al. [6], we start this section with a description of the model. The SPC-FQ water model contains three FQs located on the hydrogen and oxygen atomic sites, one Lennard–Jones site on the oxygen, and has the same internal geometry as the SPC model [22], with $r_{\mathrm{OH}} = 1.0$ Å and an H-O-H angle of 109.47°. The total energy of the SPC-FQ model for periodic systems using the Ewald sum under the tin-foil boundary condition, can be written as follows:

$$
\begin{aligned}
E_{\mathrm{total}} = & \sum_{i=1}^{N-1}\sum_{j=i+1}^{N} 4\epsilon\left[\left(\frac{\sigma}{r_{i\mathrm{O},j\mathrm{O}}}\right)^{12}-\left(\frac{\sigma}{r_{i\mathrm{O},j\mathrm{O}}}\right)^{6}\right]c(r_{i\mathrm{O},j\mathrm{O}})+E_{\mathrm{tail-LJ}} \\
& +\sum_{i=1}^{N-1}\sum_{j=i+1}^{N}\sum_{a=1}^{3}\sum_{b=1}^{3} q_{ia}q_{jb}\frac{\mathrm{erfc}(\kappa r_{ia,jb})}{4\pi\epsilon_0 r_{ia,jb}} \\
& +\frac{1}{2V\epsilon_0}\sum_{k\neq 0}^{K_{\max}}\frac{\exp(-k^2/4\kappa^2)}{k^2}\left|\sum_{i=1}^{N}\sum_{a=1}^{3} q_{ia}\exp(-i\mathbf{k}\cdot\mathbf{r}_{ia})\right|^2 \\
& -\frac{\kappa}{4\pi^{3/2}\epsilon_0}\sum_{i=1}^{N}\sum_{a=1}^{3} q_{ia}^2-\sum_{i=1}^{N}\sum_{a=1}^{2}\sum_{b=a+1}^{3} q_{ia}q_{ib}\frac{\mathrm{erf}(\kappa r_{ia,ib})}{4\pi\epsilon_0 r_{ia,ib}} \\
& +\sum_{i=1}^{N}\sum_{a=1}^{3}\left(\chi_a q_{ia}+0.5\sum_{b=1}^{3} q_{ia}q_{ib}J_{ab}(r_{ia,ib})\right)-Nu_{\mathrm{gp}} \quad , \qquad (1)
\end{aligned}
$$

where $\epsilon/k_{\mathrm{B}} = 148$ K and $\sigma = 3.176$ Å are the Lennard–Jones parameters; $r_{i\mathrm{O},j\mathrm{O}}$ is the oxygen–oxygen distance between molecule i and j; $c(r_{i\mathrm{O},j\mathrm{O}})$ is equal to 1 when $r_{i\mathrm{O},j\mathrm{O}} \leq r_{\mathrm{cut}}$ (the spherical potential truncation for Lennard–Jones interactions), or 0 otherwise; and $E_{\mathrm{tail-LJ}}$ is the usual analytical tail correction for the Lennard–Jones potential [1]. The variables V, ϵ_0, and q_{ia} are the volume of the simulation box, the permitivity of a vacuum, and the fluctuating charge on site a of molecule i. κ, erf(x), and erfc(x) are the Ewald screening parameter, and the error and complementary error functions, respectively. $\mathbf{k}$ is the reciprocal lattice vector of the periodic system defined by $\mathbf{k} = 2\pi(\mathbf{h}^{-1})^t(l\ m\ n)$, where $\mathbf{h}$ is the matrix of basis vectors of the simulation box, and l, m, and n are integers. $K_{\max}$ denotes the upper limit of the reciprocal space summation, i.e. $l^2+m^2+n^2 \leq K_{\max}^2$. χ and J are parameters determined from the ionization potential and the electron affinity and are dependent on the atom type: $\chi_{\mathrm{O}} - \chi_{\mathrm{H}} = 3.690 \times 10^4$ K, $J_{\mathrm{OO}}^{\mathrm{self}} = 1.847 \times 10^5$ K, $J_{\mathrm{HH}}^{\mathrm{self}} = 1.974 \times 10^5$ K, $J_{\mathrm{OH}}(r_{\mathrm{OH}}) = 1.389 \times 10^5$ K, and $J_{\mathrm{HH}}(r_{\mathrm{HH}}) = 9.863 \times 10^4$ K. u_{gp} is the gas-phase energy of an individual molecule.

Before describing the details of the MC algorithms introduced here for the sampling of systems with nuclear and electronic degrees of freedom, we would like to emphasize the following. These algorithms should sample the nuclear coordinates from the relevant canonical, grand-canonical, isobaric-isothermal, and Gibbs ensemble distributions (partition functions) that correspond to the BO limit. Depending on the specific ensemble and the flexibility of the molecules, different types of displacements have to be performed on nuclear coordinates including translations, rotations, conformational changes, volume changes, and molecule swap moves. While the sequential FQ (SFQ) algorithm introduces an independent electronic move that is performed sequentially before or after nuclear moves, the adiabatic nuclear and electronic MC and matrix minimization MC algorithms employ electronic moves that are performed "on-the-fly" during every type of nuclear move.

2.1 SFQ–MC algorithm

This is the algorithm described in our previous communication [21]. Starting from a given nuclear and electronic configuration, the SFQ-MC algorithm in the canonical ensemble proceeds as follows.

1. Randomly select the type of move to be attempted: (a) any type of displacement of the nuclear coordinates, or (b) electronic move, in which a set of randomly selected electronic coordinates is displaced obeying any imposed constraints (e.g. neutrality of any given molecule or neutrality of the entire system). The parameter R_{elec} determines the relative probability of selecting electronic moves over nuclear moves. In the special case of the SPC-FQ water model in the canonical ensemble, two different types of nuclear moves are used: translation and rotation of only the nuclear coordinates of a randomly selected molecule with displacements selected uniformly from the range $(-d_{\mathrm{trans}}; +d_{\mathrm{trans}})$ or $(-d_{\mathrm{rot}}; +d_{\mathrm{rot}})$. During the electronic move one of the three partial charges (on a randomly selected water molecule) is randomly selected and changed by an amount of dq selected uniformly from the range $(-d_{\mathrm{elec}}; +d_{\mathrm{elec}})$, while the other two charges are changed by $-dq/2$, if the neutrality constraint is imposed on each individual molecule.
2. Calculate the energy difference, ΔE, between the trial and old configuration.
3. Accept/reject the trial move using the Metropolis acceptance criterion with temperature T for nuclear moves and temperature T_{elec} for electronic moves.
4. Go back to step 1.

2.2 Adiabatic nuclear and electronic sampling MC (ANES-MC) algorithm

Starting from a given nuclear and electronic configuration, the ANES-MC algorithm proceeds as follows.

1. Attempt any type of displacement of nuclear coordinates (e.g. a translation or rotation of the nuclear coordinates of a randomly selected molecule with uniformly selected displacements).
2. Attempt R_{elec} electronic moves on randomly selected electronic degrees of freedom (see Sect. 6 for a discussion on preferential selection of specific electronic degrees of freedom) and conditionally accept/reject each of these electronic moves using the standard Metropolis acceptance rule with temperature T_{elec}.
3. Accept/reject the combined nuclear/electronic move (steps 1 and 2) using the standard Metropolis acceptance rule with temperature T. If rejected, return to the old nuclear and electronic configuration.
4. Go back to step 1.

While the SFQ-MC algorithm sequentially performs either nuclear or electronic moves which might favor the initial state over the trial state in a nuclear move, the ANES-MC algorithm is designed to avoid this danger by performing a simultaneous update of the electronic configuration during every nuclear move. It is easy to demonstrate that under the condition that $R_{\mathrm{elec}} \to \infty$ and $T_{\mathrm{elec}} \to 0$ K, the ANES-MC will find the electronic ground state (BO surface) by a simulated annealing process.

2.3 Matrix-minimization MC (MM-MC) algorithm

Starting from a given nuclear and ground-state electronic configuration, the MM-MC algorithm proceeds as follows.

1. Attempt any type of displacement of nuclear coordinates (e.g. a translation or rotation of the nuclear coordinates of a randomly selected molecule with uniformly selected displacements).
2. Find the electronic ground state for the new nuclear configuration by the MM method (see later).
3. Accept/reject the nuclear move using the standard Metropolis acceptance rule with temperature T.
4. Go back to step 1.

Any configuration visited by the MM-MC method lies on the BO surface, and the MM-MC method therefore samples from the correct BO distribution. The results given by this method will be the standard when analytical solutions are not available.

The details of the MM-MC method applied to the SPC-FQ water model are as follows. In the MM-MC method, the charges are functions of the nuclear coordinates. Under the constraint of neutrality imposed on each molecule, the charges can be solved using the method of Lagrange undetermined multipliers to minimize the following energy functional:

$$\mathscr{U} = E_{\text{total}} + \sum_{i=1}^{N} \lambda_i \sum_{a=1}^{3} q_{ia} \tag{2}$$

which is to solve a set of linear equations:

$$\begin{aligned}\frac{\partial \mathscr{U}}{\partial q_{ia}} = & \sum_{j=1,j\neq i}^{j=N} \sum_{b=1}^{3} \frac{q_{jb}\operatorname{erfc}(\kappa r_{ia,jb})}{4\pi\epsilon_0 r_{ia,jb}} \\ & + \frac{1}{V\epsilon_0} \sum_{k\neq 0}^{K_{\max}} \frac{\exp(-k^2/4\kappa^2)}{k^2} \sum_{j=1}^{N} \sum_{b=1}^{3} q_{jb} \cos(\mathbf{k}\cdot\mathbf{r}_{ia,jb}) \\ & + \sum_{b=1}^{3} q_{ib} \left(J_{ab} - \frac{\operatorname{erf}(\kappa r_{ia,ib})}{4\pi\epsilon_0 r_{ia,ib}} \right) \\ & - \frac{\kappa}{2\pi^{3/2}\epsilon_0} q_{ia} + \lambda_i + \chi_a = 0 \end{aligned} \tag{3a}$$

$$\frac{\partial \mathscr{U}}{\partial \lambda_i} = \sum_{a=1}^{3} q_{ia} = 0 \ . \tag{3b}$$

The above matrix equation can be solved using the Lapack subroutine called dgesv.

3 Model problems

3.1 xy problem

Recently, Martyna and Klein [unpublished work] have introduced a simple model problem consisting of two coupled oscillators to test thermostating algorithms used for adiabatic molecular dynamics simulations. The potential function of the model system is

$$E(x,y) = \frac{1}{2}(x-y)^2 + \frac{1}{2}x^2 \ . \tag{4}$$

There are two coupled degrees of freedom: x (the nuclear) and y (the electronic), with two different (kinetic) temperatures, $T = 1.0$ and $T_{\text{elec}} = 0.01$. Under the appropriate adiabatic (BO) limit (x motion slow, y motion fast), the probability distributions of x and y are identical and are given by the following functions:

$$P(x) = \frac{1}{\sqrt{2T\pi}} \exp\left(-\frac{x^2}{2T}\right) \tag{5a}$$

$$P(y) = \frac{1}{\sqrt{2T\pi}} \exp\left(-\frac{y^2}{2T}\right) \ . \tag{5b}$$

The inverse limit is approached when y moves much more slowly than x. In the inverse limit, the distributions of x and y are no longer identical:

$$P(x) = \frac{1}{\sqrt{T\pi}} \exp\left(-\frac{x^2}{T}\right) \tag{6a}$$

$$P(y) = \frac{1}{\sqrt{4T_{\text{elec}}\pi}} \exp\left(-\frac{y^2}{4T_{\text{elec}}}\right) \ . \tag{6b}$$

Martyna and Klein have shown that using a knotted Nosé–Hoover thermostat [23], the BO limit and inverse limit are sampled correctly for masses of $m_x = 1$, $m_y = 0.001$ and $m_x = 1$, $m_y = 1000$, respectively, whereas, a conventional Nose–Hoover thermostat [24, 25] fails to achieve the correct probability distributions. The time step, the kinetic temperature, and the (fictitious) masses of the electronic degrees of freedom are the parameters that have to be adjusted in molecular dynamics simulations to achieve the adiabatic separation of electronic and nuclear degrees of freedom. Neither time step nor masses are relevant parameters in a MC simulation. However, the MC parameters R_{elec} (the ratio of electronic versus nuclear moves in SFQ-MC or the number of electronic moves performed during every nuclear move in ANES-MC), and the maximum displacements for the translation of the x and y coordinates (d_x and d_y) play an equivalent role.

First, using $d_x = 0.1$ the effects of varying R_{elec} and d_y [the two parameters that describe the sampling of the (electronic) y coordinate] on the adiabatic sampling of the SFQ-MC algorithm were investigated. Comparisons of probability distributions for the x and y coordinates obtained from the SFQ-MC simulations to the analytical solutions for the BO and inverse limits are shown in Figs. 1 and 2. It is evident that there is a cooperative effect: larger R_{elec} and larger d_y (resulting in $R_{\text{elec}} d_y \gg d_x$) together help to reach the BO limit, while smaller values (resulting in $R_{\text{elec}} d_y \ll d_x$) help to achieve the inverse limit. Here it should be pointed out that too large d_y will lead to very small acceptance rates and the sampling of the adiabatic limit will deteriorate. The (fictitious) electronic mass utilized in molecular dynamics simulations to reach the adiabatic limit actually corresponds to two parameters (R_{elec} and d_y) in the SFQ-MC algorithm.

Careful examination of Figs. 1 and 2, however, reveals that the BO limit was only closely approached using a suitable combination of R_{elec} and d_y for the large maximum displacement of the (nuclear) x coordinate, $d_x = 0.1$. Low-energy states are slightly favored resulting in a slightly narrower distribution than the BO limit. This small deviation is related to the problem mentioned earlier. The sequential nature of the SFQ-MC algorithm might favor the initial state over the trial state in moves of the (nuclear) x coordinate, since the initial state is more likely to have a lower energy because its y coordinate has been sampled in previous electronic moves. A better demonstration is given by the

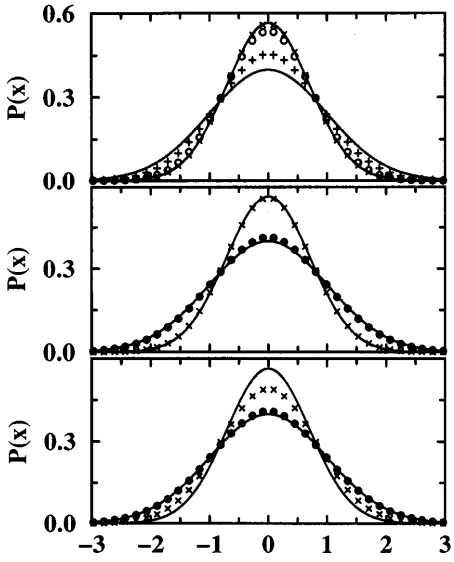

Fig. 1. Probability distribution of the x coordinate obtained with the sequential fluctuating charge–Monte Carlo (*SFQ-MC*) algorithm for the xy problem when $d_x = 0.1$. *Solid lines* represent the Born–Oppenheimer (*BO*) (*lower* and *wider*, Eq. 5a) and inverse (*higher* and *narrower*, Eq. 6a) limits. *Crosses*, *circles*, and *plusses* denote results for $d_y = 0.001$, 0.1, and 10, respectively. *Top*, *middle*, and *bottom* panels show results for $R_{\text{elec}} = 0.01$, 1, and 100, respectively

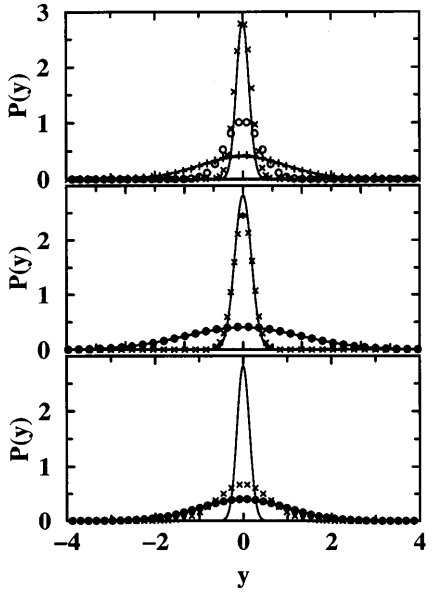

Fig. 2. Probability distribution of the y coordinate obtained with the SFQ-MC algorithm for the xy problem when $d_x = 0.1$. *Solid lines* represent the BO (*lower* and *wider*, Eq. 5b) and inverse (*higher* and *narrower*, Eq. 6b) limits. *Crosses*, *circles*, and *plusses* denote results for $d_y = 0.001$, 0.1, and 10, respectively. *Top*, *middle*, and *bottom* panels show results for $R_{\text{elec}} = 0.01$, 1, and 100, respectively

following four-state xy problem: states α ($x = 0$, $y = 0$) and β ($x = 1$, $y = 1$) are on the BO surface, state γ ($x = 1$, $y = 0$) and δ ($x = 0$, $y = 1$) are two transition states for the transfer between α and β. In the SFQ-MC algorithm there is no direct path between α and β, T is used only for moves of the x coordinate, while T_{elec} is used for y. In the BO limit, it should be expected that $P_\alpha/P_\beta = \exp[1/2T]$; however, the SFQ-MC algorithm yields a ratio of $\exp[1/T]$, thus greatly favoring the low-energy state α.

The obvious question is whether this favoring of low-energy states is related to the maximum displacement used for the (nuclear) x coordinate; thus, we have investigated the effect of d_x on the x and y distribution using $R_{\text{elec}} = 100$ and $d_y = d_x$. The probability distributions of x are shown in Fig. 3. It is obvious that smaller values of d_x allow one to approach the BO limit. Thereafter, we used a very large value for the nuclear displacement ($d_x = 1$) and varied d_y (Fig. 3). For this value of d_x, no value of d_y allows a satisfactory sampling of the adiabatic limit; thus, the importance of the maximum displacement for the nuclear degrees of freedom is evident. This is similar to what is observed in molecular dynamics simulations [10, 17], where the choice of the time step is also very important. The maximum displacement for nuclear coordinates in the SFQ-MC algorithm is limited by the skin thickness of the BO surface (which is roughly the magnitude of the electronic temperature times the number of electronic degrees of freedom).

Can the sampling problem caused by large nuclear displacements be avoided? The ANES-MC algorithm averts this problem by performing R_{elec} electronic moves on the nuclear trial configuration, thereby allowing the system to reach an equilibrium electronic configuration. As demonstrated by statistical-mechanical arguments in Sect. 7, the "instantaneous" probability to visit a nuclear configuration is not exactly that corresponding to the BO limit, but the "average" probability agrees

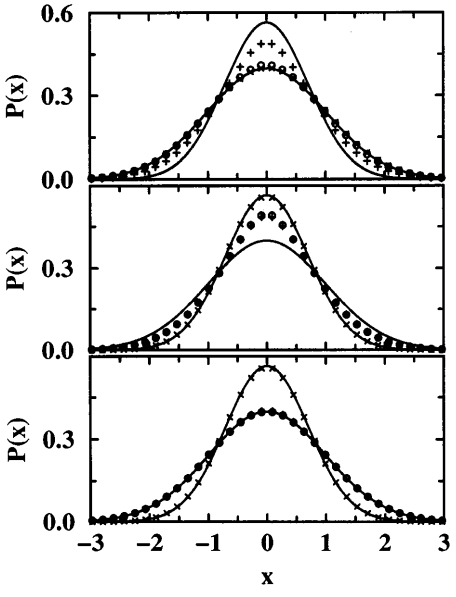

Fig. 3. Probability distribution of the x coordinate for the xy problem. (*Top*) Using the SFQ-MC algorithm with $R_{\text{elec}} = 10$. *Crosses*, *circles*, and *plusses* denote the results for $d_x = d_y = 0.01$, 0.1, and 1, respectively. Using the SFQ-MC (*middle*) or ANES-MC (*bottom*) algorithms with $d_x = 1$ and $R_{\text{elec}} = 100$. *Crosses*, *circles*, and *plusses* denote results for $d_y = 0.001$, 0.1, and 10, respectively. *Solid lines* represent the BO (*lower* and *wider*) and inverse (*higher* and *narrower*) limits

with the BO limit to high accuracy under the following conditions:

1. The electronic configurations of both initial and trial nuclear configurations are within the skin thickness of the BO surface.
2. The electronic configuration is sampled from its correct distribution.
3. The BO skin thickness is made sufficiently small by using a low electronic temperature when the electronic degrees of freedom are coupled in a nonquadratic formula.

In this case, the probability to visit a nuclear configuration will fluctuate (caused by the fast electronic motion) around the correct BO limit, in a similar fashion as the electronic forces on the nuclei fluctuate around the correct BO limit in the Car–Parrinello molecular dynamics method.

Numerical results for the *xy* problem obtained using the ANES-MC algorithm are shown in Fig. 3. As can be seen, the ANES-MC algorithm yields the correct BO limit even for large d_x, if the combination of R_{elec} and d_y allows the system to reach the BO surface. Here it should be mentioned that the average energy of the *xy* system was found to be $0.5T + 0.5T_{\text{elec}}$ (in dimensionless units), as should be expected for two (uncoupled) harmonic oscillators at temperatures T and T_{elec} (see also Sect. 6).

3.2 *AaBb* problem

The *xy* problem contains only one nuclear and one electronic degree of freedom, thus every electronic move samples all electronic degrees of freedom. Further numerical tests were performed on a system containing two nuclear (A and B) and two electronic (a and b) degrees of freedom that are all coupled. Again, the nuclear and electronic temperatures are set to $T = 1$ and $T_{\text{elec}} = 0.01$ (in dimensionless units). The potential function of the *AaBb* system is given by

$$E = \frac{1}{2}\left[A^2 + B^2 - (A-B)^2 + (A-a)^2 + (A-b)^2 + (B-a)^2 + (B-b)^2 + (a-b)^2\right] . \tag{7}$$

In the BO limit, both electronic coordinates will be the average nuclear position, $(A+B)/2$. The coordinate probability distributions are as follows:

$$P(A) = \frac{1}{\sqrt{2T\pi}}\exp\left(-\frac{A^2}{2T}\right) \tag{8a}$$

$$P(B) = \frac{1}{\sqrt{2T\pi}}\exp\left(-\frac{B^2}{2T}\right) \tag{8b}$$

$$P(a) = \frac{1}{\sqrt{T\pi}}\exp\left(-\frac{a^2}{T}\right) \tag{8c}$$

$$P(b) = \frac{1}{\sqrt{T\pi}}\exp\left(-\frac{b^2}{T}\right) . \tag{8d}$$

The maximum displacements for the nuclear coordinates ($d_A = d_B = 0.1$ or 1) are again the focus of our investigation. The distributions of A are compared in Fig. 4.

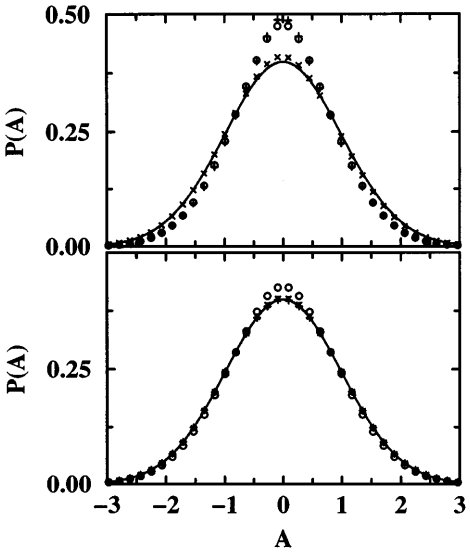

Fig. 4. Probability distribution of the A coordinate for the *AaBb* problem using the SFQ-MC (*top*) and ANES-MC (*bottom*) algorithms. *Solid lines* represent the BO limit. Simulation results using $d_A = d_B = d_a = d_b = 0.1$, $R_{\text{elec}} = 10$ (*crosses*), $d_A = d_B = d_a = d_b = 1$, $R_{\text{elec}} = 10$ (*circles*), and $d_A = d_B = 1$, $d_a = d_b = 0.1$, $R_{\text{elec}} = 100$ (*plusses*) are shown

Again, the SFQ-MC algorithm does not sample the adiabatic limit for large maximum displacements, while the ANES-MC algorithm yields the desired distributions when sufficient numbers of electronic moves are performed (where the sufficient number depends on the maximum nuclear displacement). Furthermore, the average energy obtained using the ANES-MC algorithm is close to $T + T_{\text{elec}}$.

4 SPC-FQ water dimer

The numerical results for the two simple model problems consisting of coupled harmonic oscillators have demonstrated that the ANES-MC algorithm is able to yield adiabatic sampling and that the SFQ-MC algorithm can suffer from sampling problems caused by large nuclear displacements; however, these model problems can only serve as the first test of sampling algorithms for complex molecular systems. Next, we chose to study a confined water dimer using the SPC-FQ force field [6].

Two water molecules were put in a cubic box with a linear dimension of 15 Å. Periodic boundary conditions and the minimum-image convention for all nonbonded interactions were used. Following from Eq. (1), the total energy of the SPC-FQ water dimer, using the Ewald sum with the tin-foil boundary condition, can be obtained from

$$E_{\text{dimer}} = 4\epsilon\left[\left(\frac{\sigma}{r_{1\text{O},2\text{O}}}\right)^{12} - \left(\frac{\sigma}{r_{1\text{O},2\text{O}}}\right)^{6}\right] + \sum_{a=1}^{3}\sum_{b=1}^{3} q_{1a}q_{2b}\frac{\operatorname{erfc}(\kappa r_{1a,2b})}{4\pi\epsilon_0 r_{1a,2b}}$$

$$+\frac{1}{2V\epsilon_0}\sum_{k\neq 0}^{K_{\max}}\frac{\exp(-k^2/4\kappa^2)}{k^2}$$
$$\times\left|\sum_{i=1}^{2}\sum_{a=1}^{3}q_{ia}\exp(-i\mathbf{k}\cdot\mathbf{r}_{ia})\right|^2$$
$$-\frac{\kappa}{4\pi^{3/2}\epsilon_0}\sum_{i=1}^{2}\sum_{a=1}^{3}q_{ia}^2$$
$$-\sum_{i=1}^{2}\sum_{a=1}^{2}\sum_{b=a+1}^{3}q_{ia}q_{ib}\frac{\mathrm{erf}(\kappa r_{ia,ib})}{4\pi\epsilon_0 r_{ia,ib}}$$
$$+\sum_{i=1}^{2}\sum_{a=1}^{3}\left(\chi_a q_{ia}+0.5\sum_{b=1}^{3}q_{ia}q_{ib}J_{ab}(r_{ia,ib})\right)-2u_{\mathrm{gp}}\,. \tag{9}$$

In the MM-MC method, the values of the fluctuating charges are found using the matrix equation $\mathbf{A}\times\mathbf{X}=\mathbf{B}$, where $\mathbf{A}$ is an 8×8 matrix and $\mathbf{B}$ is an 8×1 vector; both $\mathbf{A}$ and $\mathbf{B}$ are input data that are calculated using Eq. (3); the vector $\mathbf{X}$ is the output containing the ground-state charges and the two Lagrange multipliers. Once the ground-state electronic configuration is solved, the dimer energy can be directly calculated from

$$E_{\mathrm{dimer}}=4\epsilon\left[\left(\frac{\sigma}{r_{1\mathrm{O},2\mathrm{O}}}\right)^{12}-\left(\frac{\sigma}{r_{1\mathrm{O},2\mathrm{O}}}\right)^{6}\right]$$
$$+0.5\sum_{i=1}^{2}\sum_{a=1}^{3}\chi_a q_{ia}^{\mathrm{BO}}-2u_{\mathrm{gp}}\ , \tag{10}$$

where q_{ia}^{BO} is the value of the charge on site a of molecule i in its ground-state electronic configuration. The MM-MC method was applied to the water-dimer problem to obtain the standard for the later comparison with the ANES-MC algorithm. The nuclear temperature was set to 298 K. The maximum displacements for translations and rotations were set to 7 Å and 3 rad, resulting in acceptance rates of approximately 77%. The canonical ensemble averages were calculated using 2×10^7 configurations. The average dimer energy is $-(457.7\pm 1.4)$ K, where the standard error of the mean is obtained by dividing the simulation into ten blocks. The resulting charge distributions are shown in Fig. 5. There are sharp peaks in the oxygen and hydrogen charge distributions at values close to the ground-state, gas-phase charges. The shoulders are caused by the formation of dimers. Radial distribution functions (RDFs) are presented in Fig. 6. There is a sharp peak in the oxygen–oxygen RDF at 3.06 Å, a sign of strongly associating dimers. This room-temperature value is slightly larger than that of the minimum-energy SPC-FQ water dimer (2.94 Å) [6].

Thereafter, the ANES-MC algorithm was used for simulations of the SPC-FQ water dimer following similar procedures as used for the *xy* and *AaBb* model systems. First, the maximum displacements for the nuclear motions were set to the same values as used for the MM-MC simulation. The maximum displacement for the electronic move on the FQs was set to 0.03 e.

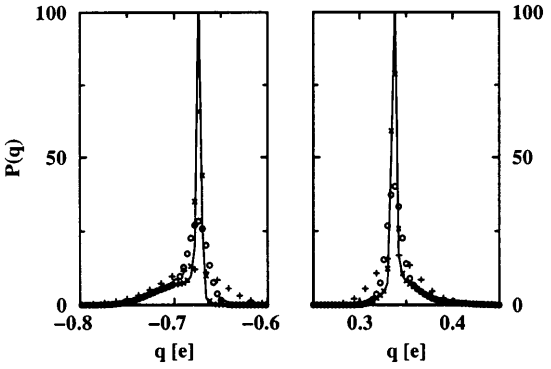

Fig. 5. Oxygen (*left*) and hydrogen (*right*) charge distributions for the *SPC-FQ* dimer ($T=298$ K, $\rho=0.0177$ g/ml) calculated with the adiabatic nuclear and electronic sampling MC (*ANES-MC*) algorithm using $R_{\mathrm{elec}}=1000$ and $T_{\mathrm{elec}}=0.5$ K (*crosses*), 5 K (*circles*), and 50 K (*plusses*). *Solid lines* represent the charge distributions obtained using the matrix-minimization MC (*MM-MC*) method

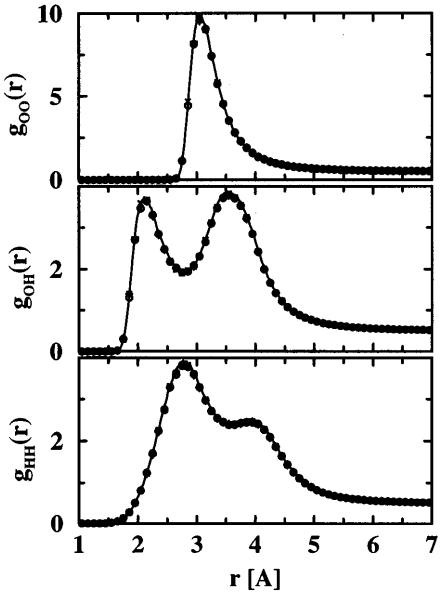

Fig. 6. Oxygen–oxygen (*top*), oxygen–hydrogen (*middle*), and hydrogen–hydrogen (*bottom*) radial distribution functions for the SPC-FQ dimer ($T=298$ K, $\rho=0.0177$ g/ml) calculated with the ANES-MC algorithm using $R_{\mathrm{elec}}=1000$ and $T_{\mathrm{elec}}=5$ K (*circles*) and 50 K (*plusses*). *Solid lines* represent the radial distribution functions obtained using the MM-MC method

Different values were explored for the electronic temperature ($T_{\mathrm{elec}}=0.5$, 5, 10, and 50 K) and the number of electronic moves ($R_{\mathrm{elec}}=50$ and 1000). For each combination of T_{elec} and R_{elec} parameters, the ANES-MC simulation results were averaged over 10^7 configurations. The average dimer energies, $\langle E_{\mathrm{dimer}}\rangle$, obtained for $T_{\mathrm{elec}}=0.5$ K are $-(460.2\pm 2.1)$ K ($R_{\mathrm{elec}}=50$) and $-(459.5\pm 2.1)$ K ($R_{\mathrm{elec}}=1000$), were in good agreement with the adiabatic limit obtained from the MM-MC simulations. For both R_{elec} values, the $\langle E_{\mathrm{dimer}}\rangle$ agree with each other for all electronic temperatures. $\langle E_{\mathrm{dimer}}\rangle$ is plotted against T_{elec} in Fig. 7. As already

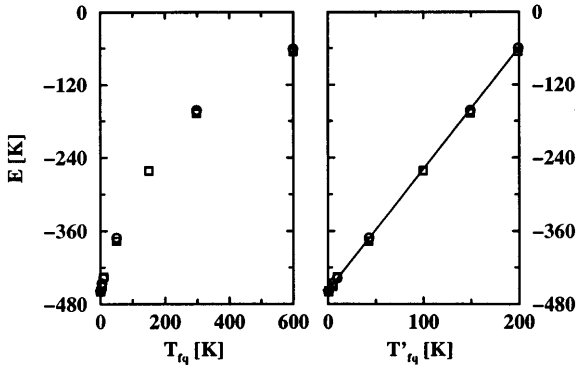

Fig. 7. Average dimer energy for the SPC-FQ model calculated with the ANES-MC algorithm versus T_{elec} (*left*) or T'_{elec} (*right*) for $R_{\text{elec}} = 50$ (*squares*) and 1000 (*circles*). The average dimer energy calculated using the MM-MC method is depicted as a *star* at 0 K. A linear fit of the average dimer energy versus T'_{elec} for the $R_{\text{elec}} = 1000$ results is also shown

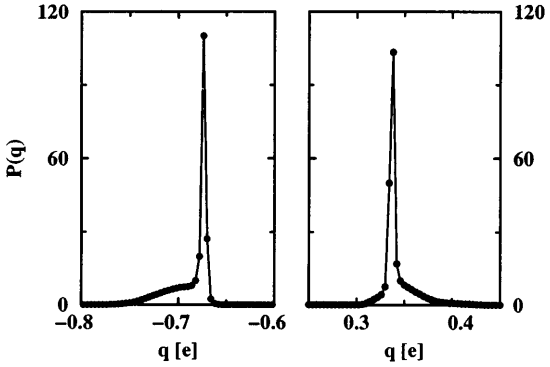

Fig. 8. Oxygen (*left*) and hydrogen (*right*) charge distribution for the SPC-FQ dimer ($T = 298$ K, $\rho = 0.0177$ g/ml) calculated with the ANES-MC algorithm using $R_{\text{elec}} = 5000$ and $T_{\text{elec}} = 0.001$ K (*circles*), and calculated with the MM-MC method (*solid line*)

demonstrated for the two harmonic-oscillator problems, $\langle E_{\text{dimer}} \rangle$ calculated using the ANES-MC algorithm can be approximated by $\langle E_{\text{BO}} \rangle + 0.5 N_{\text{elec}} T_{\text{elec}}$, where $\langle E_{\text{BO}} \rangle$ is the average energy corresponding to the BO limit (which can be calculated using the MM-MC method) and N_{elec} is the total number of electronic degrees of freedom with a kinetic temperature of T_{elec}. This formula works well for the SPC-FQ water dimer, except that there is a larger deviation for $T_{\text{elec}} = 50$ K. As demonstrated in Sect. 7, $\langle E_{\text{dimer}} \rangle$ can be approximated by $\langle E_{\text{BO}} \rangle + 0.5 N_{\text{elec}} T_{\text{elec}}$ only at $T_{\text{elec}} \ll T$. For higher T_{elec}, $\langle E_{\text{dimer}} \rangle = \langle E_{\text{BO}} \rangle + 0.5 N_{\text{elec}} T'_{\text{elec}}$ with $T'^{-1}_{\text{elec}} = T^{-1} + T^{-1}_{\text{elec}}$.

The oxygen and hydrogen charge distributions and RDFs (for $R_{\text{elec}} = 1000$) are compared to those given by the MM-MC method in Figs. 5 and 6. Large differences are observed for the charge distributions, where increasing T_{elec} results in a broadening, in particular, for the monomer peak. Surprisingly, even at $T_{\text{elec}} = 0.5$ K the ANES-MC and MM-MC distributions are still discernible. However, despite the different charge distributions (and also average dimer energies) all RDFs agree rather well. For charge distributions and RDFs there are no significant differences between simulations using different numbers of electronic moves. Results for $R_{\text{elec}} = 50$ are therefore not included in Figs. 5 and 6. For the moment, we may conclude that 50 electronic moves are sufficient for the SPC-FQ water dimer to equilibrate the electronic degrees of freedom and to find a set of charges representative of the skin thickness of the BO surface (see also Sect. 6).

In order to demonstrate the point that under the conditions that $R_{\text{elec}} \to \infty$ and $T_{\text{elec}} \to 0$, the ANES-MC algorithm results in a simulated annealing of the electronic degrees of freedom and becomes equivalent to the MM-MC method, a simulation was carried out using ANES-MC with $T_{\text{elec}} = 0.001$ K, $R_{\text{elec}} = 5000$, and $d_{\text{elec}} = 0.0001$ e. The average dimer energy is $-(459.3 \pm 2.7)$ K. The charge distributions are plotted in Fig. 8, and are evidently indistinguishable from those obtained with the MM-MC method.

5 SPC-FQ liquid water

The numerical results for the SPC-FQ dimer system, a problem including rather complex coupling between the electronic and nuclear degrees of freedom, convincingly showed that the ANES-MC algorithm is able to be applied to common polarizable force fields and to provide reliable answers compared to the MM-MC method. Several questions remain to be answered. Will the ANES-MC algorithm work for bulk phases, where many hundreds of electronic and nuclear degrees are coupled? Will the ANES-MC algorithm be more efficient for bulk systems than the MM-MC method or the conventional iterative schemes?

Again, the MM-MC method was employed to obtain results for canonical sampling on the BO surface and to set the standard for comparison with the ANES-MC algorithm. To our knowledge, MM methods have not yet been applied to entire bulk systems. Medeiros and Costas [15] applied a MM technique in a MC simulation of polarizable water systems to update the electronic structure of only the molecule that is being displaced during the nuclear move. They argued that a full MM of the electronic structure of the entire system would be prohibitively expensive. Updating only the electronic structure of the moving molecule does not ensure sampling of the correct adiabatic limit since polarizability is a many-body effect. The detailed balance condition might be violated because the electronic structure of the moving molecule is optimized for the trial state (after the MM), but not for the old state. We wrote a special-purpose program tailored solely for MM-MC simulations of SPC-FQ water and found that it is feasible to perform simulations for systems containing a few hundred water molecules (e.g. 100 MC cycles for 100 water molecules can be carried out in approximately 1 h on an IBM RISC 604e processor). There are two components in our MM-MC program that dominate the computing requirements: calculating all elements for the matrix (see Eq. 3) and solving the matrix equation. For every MC cycle (N moves per cycle), the computing time spent on the first component scales as $\mathcal{O}(N^2 N_k)$, where N and N_k are the number of molecules and the number of recip-

rocal lattice vectors in the Ewald sum, respectively, while the computing time spent on the second component scales as $\mathcal{O}(N^4)$. In our canonical ensemble simulations, we used $N = 100$ and $N_k = 500$, and the second component is computationally more expensive. Once the ground-state electronic configuration has been found, the total energy can be simply calculated as follows:

$$E_{\text{total}} = E_{\text{LJ}} + 0.5 \sum_{i=1}^{N} \sum_{a=1}^{3} \chi_a q_{ia}^{\text{BO}} - N u_{\text{gp}} \quad . \tag{11}$$

Canonical-ensemble simulations were carried out for a system containing 100 SPC-FQ water molecules at the thermodynamic conditions of $T = 298$ K and $\rho = 1.0$ g/ml. The periodic box has a linear dimension of 14.4 Å, sufficient to investigate the third and fourth solvation shells. In the MM-MC simulation, the maximum translational and rotational displacements were set to 0.3 Å and 0.4 rad, resulting in acceptance rates of 47 and 46%, respectively. More than 25,000 MC cycles were used to equilibrate the system, and an additional 25,000 MC cycles were carried out for the production period. The average potential energy was $-(41.1 \pm 0.2)$ kJ/mol, in good agreement with the molecular dynamics results of -41.4 kJ/mol obtained by Rick et al. [6] for the SPC-FQ model. It should be mentioned that the molecular dynamics simulation was carried out for a system consisting of 256 molecules, but without tail correction for the Lennard–Jones interactions. This agreement is rather encouraging and is a first indication that the much larger differences reported in our previous communication [21] are indeed caused by the different treatment of the long-range electrostatic interactions (Ewald sum versus molecule-based spherical truncation at $r_{\text{OO}} > 10.5$ Å). The average molecular dipole moment obtained from the MM-MC simulations is 2.80 D, again in good agreement with the molecular dynamics result of 2.83 D [6]. The charge distributions are shown in Fig. 9. Compared to the charge distributions for the water dimer, the bulk charges are shifted to larger values (in magnitude), and the monomer peak has disappeared. The large enhancement in the average dipole moment of bulk liquid water compared to the water dimer emphasizes the importance of the polarization effect. The large widths of the charge distributions are caused by the locally heterogeneous water environment. The RDFs are shown in Fig. 10. The first peak of the oxygen-oxygen RDF is centered around 2.75 Å, due to the formation of strong hydrogen bonds. This value is slightly smaller than the experimental estimate of 2.82 Å [26]. Following the first peak, a long plateau ranging from 3.2 to 4.6 Å is found. This feature is quite different from the neutron-diffraction data [26], which predicted a pronounced minimum at 3.3 Å. Nevertheless, a similar plateau was also observed in the molecular dynamics simulations [6], and overall structural agreement between MM-MC and molecular dynamics simulations is very good.

The tests for the ANES-MC algorithm were performed for the same water system of 100 water molecules. First, simulations were carried out using the same set of maximum translational and rotational displacements as for the MM-MC simulations and $d_{\text{elec}} = 0.03$ e. Two different R_{elec} values (300 and 2000) were investigated using $T_{\text{elec}} = 5$ K (the standard choice in molecular dynamics simulations). The simulations were started from an equilibrated configuration obtained by the MM-MC method, and the production periods consisted of 10,000 MC cycles. The average energies were -42.6 kJ/mol ($R_{\text{elec}} = 300$) and -40.9 kJ/mol ($R_{\text{elec}} = 2000$). Compared to the MM-MC results, smaller R_{elec} yield a lower energy. This is probably caused by insufficient equilibration of the electronic configuration during the nuclear moves. This may lead to the same problem observed for the SFQ-MC algorithm, i.e. favoring of the old over the trial configuration and thus favoring of low-energy states; however, $R_{\text{elec}} = 2000$ appears to provide

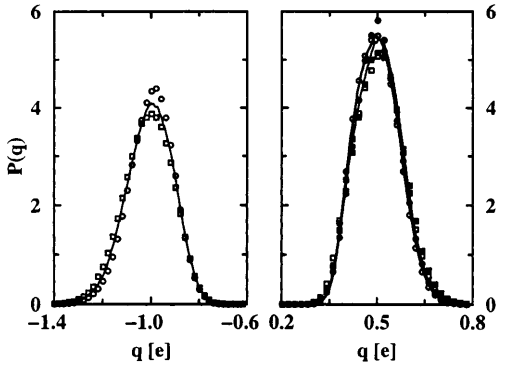

Fig. 9. Oxygen (*left*) and hydrogen (*right*; hydrogen 1: *filled symbols* and *thick line*; hydrogen 2: *open symbols* and *thin line*) charge distributions for bulk SPC-FQ water ($T = 298$ K, $\rho = 1.0$ g/ml) calculated with the ANES-MC algorithm using $R_{\text{elec}} = 2000$ and $T_{\text{elec}} = 5$ K (*circles*) and $R_{\text{elec}} = 2000$ and $T_{\text{elec}} = 50$ K (*squares*), and calculated with the MM-MC method (*solid lines*)

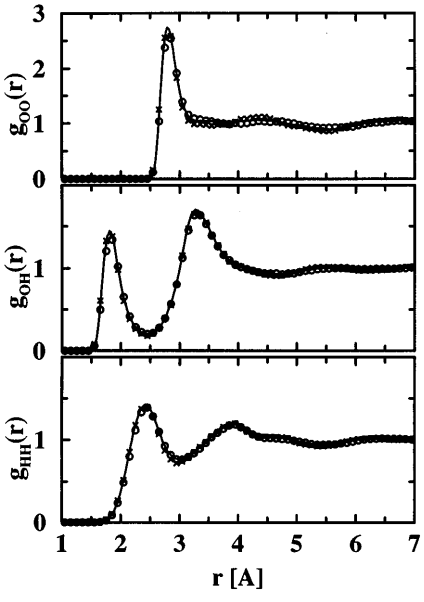

Fig. 10. Oxygen–oxygen (*top*), oxygen–hydrogen (*middle*), and hydrogen–hydrogen (*bottom*) radial distribution functions for bulk SPC-FQ water ($T = 298$ K, $\rho = 1.0$ g/ml) calculated with the ANES-MC algorithm using $R_{\text{elec}} = 2000$ and $T_{\text{elec}} = 5$ K (*circles*) and $R_{\text{elec}} = 2000$ and $T_{\text{elec}} = 50$ K (*crosses*), and calculated with the MM-MC method (*solid lines*)

sufficient sampling in this case and yields an average energy that agrees within statistical errors with the MM-MC result. The slightly higher energy (0.2 kJ/mol) may also be attributed to the motion of the electronic degrees of freedom (the thickness of the BO surface). To further investigate the contribution of the electronic motion to the total energy, an additional simulation was carried out with $R_{\mathrm{elec}} = 2000$ and $T_{\mathrm{elec}} = 50$ K. In this case, the average energy increased to -40.6 kJ/mol. The difference of $+0.5$ kJ/mol to the MM-MC result is close to what is expected for harmonic oscillators, i.e. 50 K/molecule (two electronic degrees of freedom per molecule) is equivalent to 0.4 kJ/mol. The charge distributions obtained for the two sets of FQ simulations with $R_{\mathrm{elec}} = 2000$, but with different T_{elec} are compared to those obtained by the MM-MC method in Fig. 9. The charge distributions for both T_{elec} values reproduce well those obtained for the BO limit. Compared to results for the SPC-FQ dimer, there is a much smaller dependence of the charge distributions on T_{elec}. The factor controlling the width of the charge distributions for bulk liquid water is evidently the local heterogeneity of the environment. The RDFs are compared in Fig. 10. The first and second shells of the hydrogen-bonded network are very similar for the ANES-MC and MM-MC simulations, but smaller differences can be observed beyond 4 Å, and the larger T_{elec} seems to produce a slightly more pronounced long-range structure.

From comparison of the numerical results obtained from the ANES-MC, MM-MC, and molecular dynamics simulations, it is clear that the three algorithms can be used to perform adiabatic sampling of electronic and nuclear degrees of freedom for bulk systems. However, it should be emphasized here that the ANES-MC algorithm can only work when sufficient electronic moves are performed to reach an equilibrium electronic configuration during the nuclear moves. Unlike the time-step dependence found in the molecular dynamics technique, the MM-MC and ANES-MC algorithms can (in principle) work independently of the maximum displacement of molecules during the nuclear moves; however, as discussed in Sect. 6, it may be more efficient to limit the maximum nuclear displacements in ANES-MC simulations. The rather different results for the SFQ-MC simulations reported in our previous communication [21] are mainly caused by the different treatment of long-range electrostatic interactions and partly due to the favoring of low-energy states for large maximum displacements (see Sect. 6).

6 Improving the efficiency of the ANES-MC algorithm

One important question remains open: how efficient is the ANES-MC algorithm compared to MM-MC and iterative Monte Carlo simulations for polarizable force fields? For the system of 100 water molecules studied here, using ANES-MC without any special programming effort and with $R_{\mathrm{elec}} = 2000$ is actually 3 orders of magnitude more expensive than a conventional MC simulation using the parent fixed-charge force field; however, advantage can be taken of the fact that the nuclear coordinates remain fixed during the electronic move sequence. Indeed, if all atomic separations and Ewald lattice vectors are stored, the recalculation of the energy during an electronic move can simply be performed by scaling the relevant terms. In this case (using $R_{\mathrm{elec}} = 2000$), the computational effort is only 2 orders of magnitude larger than for the fixed-charge model, i.e. comparable to the MM-MC method and iterative schemes. In the following section, it is demonstrated that the efficiency of the ANES-MC algorithm can be significantly improved by adjusting the maximum displacements used for nuclear moves.

In Car–Parrinello-type molecular dynamics simulations using the extended Lagrangian formalism, the dynamics for the nuclei and electrons are carried out in parallel. The optimization of the electronic structure is done "on-the-fly", and usually no additional time steps are used for the electronic motion that would allow the electronic structure to fall back to the BO surface. This is due to the finite skin thickness of the BO surface provided by the low electronic temperature. As long as the time step is small enough to let the nuclei move within this skin thickness, the overall Hamiltonian of the system can be approximated by an "averaged" Hamiltonian obtained by performing an average over the fast coordinates [19]. At sufficiently low electronic temperature, this "averaged" Hamiltonian will be equivalent to that corresponding to the BO limit. It is thus required that a relatively small time step (compared to a fixed-charge force field) be used to ensure that the nuclear motion does not diverge from the BO surface. Similarly, in an ANES-MC simulation we have two options: use small maximum displacements for the nuclear coordinates and remain on the BO surface, or use large displacements requiring many electronic moves to equilibrate the electronic configuration. There are two different stages during the electronic move sequence in ANES-MC that accompany every nuclear motion: first, to fall back to the skin thickness of the BO surface (most probable electronic states, not necessarily ground state); and secondly, to sample the correct electronic distribution within this skin thickness. If large maximum displacements are used for the nuclear motion, then most of the electronic moves are often spent in the first stage because the large jump requires a more drastic change in the electronic configuration. However, when the step size of the nuclear motion is small enough, the MC method will behave similarly to molecular dynamics: the nuclei are moving within the skin thickness of the BO surface provided by the low electronic temperature. No extra electronic moves need to be spent on the first stage and a few electronic moves are sufficient to sample the electronic configurations within the skin thickness. The rate of sampling the nuclear configurations might slow down for small displacements, but it should be remembered that small displacements will result in larger acceptance rates. Nevertheless, the huge gain in computational efficiency due to reducing the number of electronic moves will certainly more than compensate for the smaller nuclear displacements.

Tests of the energy evolution in the ANES-MC algorithm against the number of electronic moves were

carried out using different maximum displacements for both the SPC-FQ dimer and bulk phase. $T_{elec} = 5$ K and $R_{elec} = 2000$ were used for all simulations. It should be expected that the energy always decreases during an initial period (falling back to the BO skin thickness), followed by a fluctuation around a certain value (sampling within the BO skin thickness). The optimum number of electronic moves required in an ANES-MC simulation (for given maximum displacements) can then be determined from the point where sampling of equilibrium electronic structures starts. For the SPC-FQ dimer, two sets of maximum displacements were chosen: $d_{trans} = 7$ Å and $d_{rot} = 3$ rad, or 1 Å and 1 rad. For both cases 100,000 MC cycles were carried out. Individual and average evolutions of the dimer energy (using the energy immediately after the nuclear move, before any electronic move is performed, as the zero of energy) are plotted in Fig. 11. The evolution of the average energy shows that the larger set of maximum displacements results in a larger decrease in the energy and requires more electronic moves to reach equilibrium. Nevertheless, 50 electronic moves are sufficient to ensure that the electronic states are within the skin thickness of the BO surface. It is instructive to compare also individual energy evolutions. For the larger nuclear displacements, a very large decrease in the energy followed by random fluctuations is observed in three cases, which might correspond to cases where the nuclear move results in the formation or dissociation of a dimer. For the remaining seven evolutions shown, however, the energy fluctuates randomly from the beginning. For the smaller set of nuclear displacements, none of the individual energy evolutions show a dramatic change. The individual energies seem to fluctuate randomly almost from the beginning. This may correspond to a situation where the nuclei are always moving within the skin thickness of the BO surface.

What about the bulk phase? Three different sets of maximum displacements were investigated: $d_{trans} = 0.3$ Å and $d_{rot} = 0.4$ rad, 0.2 Å and 0.2 rad, or 0.1 Å and 0.1 rad. Fifty thousand MC moves were carried out for the 100-molecule system. The energy evolutions for the first and third sets of nuclear displacements are plotted in Fig. 12. The energy evolutions follow the same trend as for the dimer, i.e. larger nuclear displacements result in larger decreases in the energy and require more electronic moves to reach the electronic equilibrium. For the first set of maximum displacements (0.3 Å and 0.4 rad), which was also used for the simulations described in the previous section, 2000 electronic moves are barely sufficient to reach the electronic equilibrium, while 300 moves are certainly far from satisfactory. More important, however, is that by using maximum displacements of 0.1 Å and 0.1 rad, the average energy evolution is almost flat: no significant decrease is visible and the energy fluctuates right from the start for all ten individual evolutions shown. It is evident that for this set of maximum displacements, the nuclei are moving within the skin thickness of the BO surface and very few electronic moves are required. Here it should be mentioned that the acceptance rates for translational and rotational moves were 79 and 83% for this case, while 47 and 46% were observed for the larger displacements of 0.3 Å and 0.4 rad.

Further simulations were carried out for the ANES-MC algorithm using maximum displacements of 0.1 Å and 0.1 rad. T_{elec} was set to 5 K in all cases, while three R_{elec} values were used: 10, 50, and 500. The simulations were started from an equilibrated configuration, and the production periods consisted of 10,000 MC cycles.

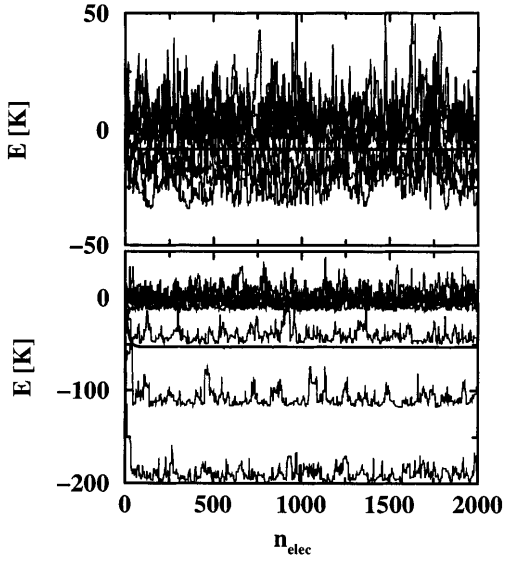

Fig. 11. Evolution of the total energy versus the number of electronic moves during an ANES-MC nuclear move for the SPC-FQ water dimer ($T = 298$ K, $\rho = 0.0177$ g/ml). The *thick line* represents the average evolution. *The thin lines* depict ten individual evolutions. (*Bottom*) $d_{trans} = 7$ Å and $d_{rot} = 3$ rad; (*top*) 1 Å and 1 rad

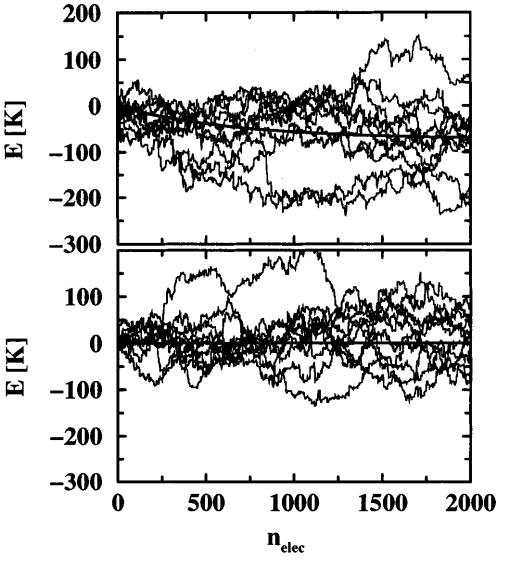

Fig. 12. Evolution of the total energy versus the number of electronic moves during an ANES-MC nuclear move for bulk SPC-FQ water ($T = 298$ K, $\rho = 1.0$ g/ml). The *thick line* represents the average evolution. The *thin lines* depict ten individual evolutions. (*Top*) $d_{trans} = 0.3$ Å and $d_{rot} = 0.4$ rad; (*bottom*) 0.1 Å and 0.1 rad)

The average potential energies were as follows: $-(41.0 \pm 0.3)$ kJ/mol ($R_{\text{elec}} = 10$), $-(41.7 \pm 0.5)$ kJ/mol ($R_{\text{elec}} = 50$), and $-(41.0 \pm 0.4)$ kJ/mol ($R_{\text{elec}} = 500$). All are in good agreement with the MM-MC result of $-(41.1 \pm 0.2)$ kJ/mol. This is a clear demonstration that by using slightly smaller maximum displacements, the number of electronic moves can be significantly reduced from 2000 to 10, while little influence on the accuracy is observed. Comparisons were also made for the charge distributions and the RDFs (Figs. 13, 14). The results obtained using the ANES-MC algorithm with small nuclear displacements and few electronic moves are indistinguishable from those obtained with the MM-MC method.

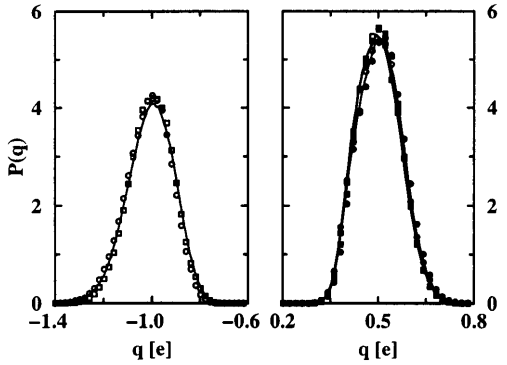

Fig. 13. Oxygen (*left*) and hydrogen (*right*; hydrogen 1: *filled symbols* and *thick line*; hydrogen 2: *open symbols* and *thin line*) charge distributions for bulk SPC-FQ water ($T = 298$ K, $\rho = 1.0$ g/ml) calculated with the ANES-MC algorithm using $d_{\text{trans}} = 0.1$ Å, $d_{\text{rot}} = 0.1$ rad, $T_{\text{elec}} = 5$ K, and $R_{\text{elec}} = 10$ (*circles*) or $R_{\text{elec}} = 500$ (*squares*), and calculated with the MM-MC method (*solid lines*)

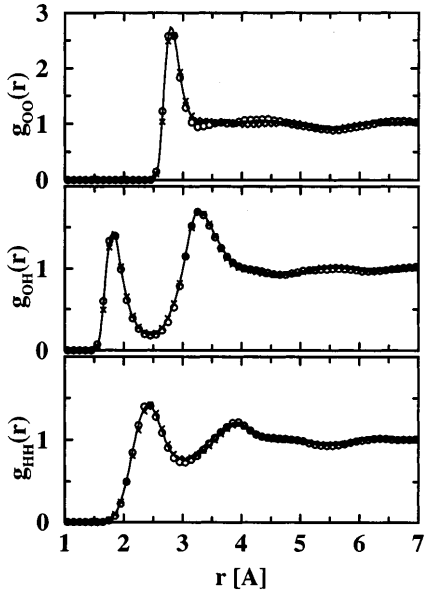

Fig. 14. Oxygen–oxygen (*top*), oxygen–hydrogen (*middle*), and hydrogen–hydrogen (*bottom*) radial distribution functions for bulk SPC-FQ water ($T = 298$ K, $\rho = 1.0$ g/ml) calculated with the ANES-MC algorithm using $d_{\text{trans}} = 0.1$ Å, $d_{\text{rot}} = 0.1$ rad, $T_{\text{elec}} = 5$ K, and $R_{\text{elec}} = 10$ (*circles*) or $R_{\text{elec}} = 500$ (*crosses*), and calculated with the MM-MC method (*solid lines*)

The results described on the energy evolution during the electronic-move period not only provide a way to design an efficient MC algorithm for polarizable force fields, but also support the fact that molecular dynamics simulations using the extended Lagrangian formalism sample the correct BO distribution under the condition of sufficiently small time steps. How will the SFQ-MC algorithm perform when small nuclear displacements are used? A SFQ-MC simulation of 20,000 MC cycles was carried out using maximum displacements of 0.1 Å and 0.1 rad, $T_{\text{elec}} = 5$ K, and $R_{\text{elec}} = 10$. In this case, the average potential energy is $-(41.2 \pm 0.1)$ kJ/mol, which is in good agreement with the MM-MC and ANES-MC results. Furthermore, the charge distributions and the RDFs also compare well with the distributions obtained using the other methods. Thus, as for the *xy* and *AaBb* systems, as long as nuclear moves do not result in a departure from the BO skin thickness, the SFQ-MC method appears to sample the desired adiabatic distribution.

However, compared to the SFQ-MC algorithm, there are more ways open to improve the efficiency of the ANES-MC algorithm and to extend it to other ensembles because it will, in principle, work irrespective of the step size. For example, force-bias sampling [27] might be combined with the ANES-MC algorithm. In most MC schemes, only one particle participates in each nuclear move. Although polarization is a many-body effect, the change in the electronic structure will be more dramatic in the vicinity of the molecule being moved. Therefore, electronic moves on the moving molecule and its neighboring molecules are more important for equilibrating the electronic configuration, than electronic moves performed on the molecules far away. Introducing a simple bias (say, $P_{\text{move}} = 1$ for the moving molecule and $P_{\text{move}} = 1/r$ for all other molecules, where r is the separation between the trial molecule and the moving molecule), for more frequent sampling of the moving molecule and its neighboring molecules, can in principle reduce the total number of the electronic moves needed in the first stage (the falling back to the BO thickness) and eliminate the system-size dependence for larger systems that might be present for the unbiased selection. Obviously, this needs to be explored further. Presently, we have also started to carry out ANES-MC simulations of SPC-FQ water in the Gibbs ensemble. Attempts to swap particles result in large disturbances in the electronic structure in both simulation boxes, and the biased selection of molecules for the electronic moves helps greatly to reduce the value of $R_{\text{elec}}^{\text{swap}}$ required to reach equilibrium electronic configurations. Biased selections should not be used during volume moves (in the isobaric–isothermal or Gibbs ensembles), since the changes in nuclear configurations are rather uniform over the entire system.

7 Statistical mechanics of adiabatic sampling of nuclear and electronic degrees of freedom

The discussion presented so far has focused on numerical tests of the SFQ-MC and ANES-MC algorithms. In

this section, we will turn our attention to a statistical-mechanical analysis of the canonical partition function for systems containing nuclear and electronic degrees of freedom with adiabatic separation. The canonical partition function of a system without electronic degrees of freedom can be written as follows:

$$Q = \mathscr{C} \int \exp\left(-\frac{E(\mathbf{r})}{k_B T}\right) \mathrm{d}\mathbf{r} \ , \tag{12}$$

where $\mathscr{C}$ is the standard constant containing the integration over momenta and the conversion factor required to relate the purely classical partition function to its quantum-mechanical equivalent. The remainder is the classical configuration integral that depends only on the set of nuclear coordinates, $\mathbf{r}$. The symbols E, k_B, and T stand for the potential energy, Boltzmann's constant, and the temperature. This partition function can be directly applied to the MM-MC method, because the electronic configuration in the BO limit is only a function of the nuclear coordinates, and thus the same holds true for E. However, in adiabatic sampling schemes employing a finite electronic temperature, there is a continuous distribution of electronic states (defined by a set of electronic coordinates, $\mathbf{q}$) for every nuclear configuration. This collection of electronic states forms a BO surface with finite skin thickness. Grouping the electronic states into levels, each electronic level with an energy of ϵ (choosing the electronic ground state as the zero of energy) will have a certain weight, $P(\epsilon)$, depending on both its energy and its degeneracy. In the *xy* problem discussed in Sect. 3.1, the electronic degree of freedom is coupled with the nuclear degree of freedom in a quadratic way; however, for every specific nuclear configuration, (where x is the only element of $\mathbf{r}$), using the linear transformation $s = x - y$ the energy can be decomposed into two parts

$$E(\mathbf{r},\mathbf{q}) \equiv E(x,y) = E_{gs}(\mathbf{r}) + 0.5s^2 \quad \text{with} \quad E_{gs}(\mathbf{r}) = 0.5x^2 \ . \tag{13}$$

The first part, E_{gs}, is the ground-state energy, and the second part turns out to be an uncoupled harmonic oscillator. Such a decomposition is independent of the nuclear coordinates. Therefore, it should be expected that the degeneracy of the electronic energy levels, $\omega(\epsilon)$, is the same for every nuclear configuration. Thus, it is easy to demonstrate that for each set of nuclear coordinates, the additional phase-space volume stemming from the electronic degrees of freedom at a certain temperature, T_{elec}, is identical and can be written as

$$Q_{elec}(T_{elec}) = \mathscr{C} \int_0^\infty \exp\left(-\frac{\epsilon}{k_B T_{elec}}\right) \omega(\epsilon) \mathrm{d}\epsilon \ . \tag{14}$$

This also holds true for the *AaBb* problem and the SPC-FQ water systems. The similarity among these systems is that the electronic degrees of freedom are coupled in a quadratic formula as follows:

$$E = \sum_{i,j=1}^{N_{elec}} a_{ij} x_i x_j + \sum_{i=1}^{N_{elec}} b_i x_i + c \ , \tag{15}$$

where N_{elec}, a_{ij}, and x_i are the total number of electronic degrees of freedom, constants (that may be functions of only the nuclear coordinates), and electronic coordinates (the constraint of neutrality has been removed and the x_i are not redundant as the q_i shown in Eq. 1), and b_i and c are constants. With the help of a linear coordinate transformation

$$x_i = \sum_{j=1}^{N_{elec}} d_{ij} s_j + e_i \tag{16}$$

the set of normal coordinates, s_1, s_2,..., $s_{N_{elec}}$, is introduced for which the energy is simply

$$E = \frac{1}{2} \sum_{i=1}^{N_{elec}} s_i^2 + E_{gs}(\mathbf{r}) \ . \tag{17}$$

For the *AaBb* problem, the following linear transformation is used:

$$s_1 = \sqrt{3}\left(a - \frac{b + A + B}{3}\right) \tag{18a}$$

$$s_2 = \sqrt{\frac{8}{3}}\left(b - \frac{A + B}{2}\right) \ . \tag{18b}$$

Then Eq. (7) can be written as

$$E = \frac{1}{2}\left(A^2 + B^2 + {s_1}^2 + {s_2}^2\right) = E_{gs}(\mathbf{r}) + \frac{1}{2}{s_1}^2 + \frac{1}{2}{s_2}^2 \ . \tag{19}$$

This equation falls into the category described by Eq. (17). Thus, similarly to the *xy* problem, the potential energy for any nuclear configuration can be decomposed into two parts: the ground-state energy, $E_{gs}(\mathbf{r})$, that is a function only of nuclear coordinates, and N_{elec} uncoupled harmonic oscillators. Consequently, the degeneracy of the electronic energy levels, $\omega(\epsilon)$, or the probability distribution of the electronic energy levels, $P(\epsilon)$, is the same for every nuclear configuration and depends only on T_{elec} and N_{elec}. To demonstrate this, the energy distributions of the SPC-FQ bulk system were calculated for three randomly chosen nuclear configurations ($T_{elec} = 5$ K). They are plotted by choosing the corresponding $E_{gs}(\mathbf{r})$ as the zero-energy point in Fig. 15. For comparison, the energy distribution of 200 uncoupled harmonic oscillators at 5 K is shown as well. It is evident that they are identical and close to a Gaussian distribution with a peak centered around 500 K ($200 \times 0.5 \times 5$ K) and a width of about 100 K (which is proportional to $\sqrt{N_{elec}} \times T_{elec}$). For identical distributions of electronic levels, the additional phase-space volume stemming from the electronic degrees of freedom is the same.

To recover the correct BO limit in adiabatic sampling of nuclear and electronic degrees of freedom, the integral of the probability distribution of $P(\mathbf{r},\mathbf{q})$ over all possible values of $\mathbf{q}$ must satisfy

$$\int P(\mathbf{r},\mathbf{q})\, d\mathbf{q} = \rho(\mathbf{r}) \tag{20a}$$

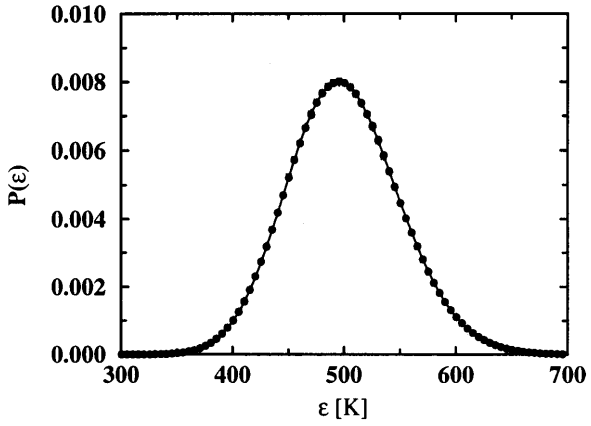

Fig. 15. Probability distributions of the electronic energy levels for bulk SPC-FQ water ($T = 298$ K, $\rho = 1.0$ g/ml) calculated with the ANES-MC algorithm using $T_{\text{elec}} = 5$ K at three randomly chosen nuclear configurations (shown as *plusses*, *circles*, and *crosses*, respectively). The distribution calculated for 200 uncoupled harmonic oscillators at 5 K is shown as a *solid line*

$$\rho(\mathbf{r}) = \exp\left[-\frac{E_{\text{gs}}(\mathbf{r})}{k_{\text{B}}T}\right] \Big/ \int \exp\left[-\frac{E_{\text{gs}}(\mathbf{r})}{k_{\text{B}}T}\right] d\mathbf{r} \tag{20b}$$

as given by Eq. (12).

To find the probability distribution $P(\mathbf{r}, \mathbf{q})$, the superdetailed balance condition is used. Let us compare any two states linked by the Markov chain, the old state Γ_1, with coordinates $(\mathbf{r_1}, \mathbf{q_1})$, and with the ground-state energy E_1 and the electronic energy ϵ_1, and the new state Γ_2, with coordinates $(\mathbf{r_2}, \mathbf{q_2})$, and with the ground-state energy E_2 and the electronic energy ϵ_2. In the ANES-MC algorithm, the probability of accepting the combined nuclear/electronic move is

$$\text{acc}(\Gamma_1 \to \Gamma_2) = \min\left[1, \exp\left(-\frac{E_2 - E_1}{k_{\text{B}}T}\right)\right] \ . \tag{21}$$

Unlike the conventional Metropolis sampling, the underlying matrix of the Markov chain is not symmetric for the ANES-MC algorithm. This is due to the fact that the probability of generating a specific electronic configuration does depend on its energy and thus the probability of generating the reverse electronic move will be different. The probability of generating the electronic configuration $\mathbf{q_2}$ at the nuclear configuration $\mathbf{r_2}$ is determined by the electronic moves

$$T_{\mathbf{r}_2}(\mathbf{q_2}) = \exp\left(-\frac{\epsilon_2}{k_{\text{B}}T_{\text{elec}}}\right) \times Q_{\text{elec}}^{-1}(\mathbf{r_2}, T_{\text{elec}}) \tag{22}$$

and for the reverse move,

$$T_{\mathbf{r}_1}(\mathbf{q_1}) = \exp\left(-\frac{\epsilon_1}{k_{\text{B}}T_{\text{elec}}}\right) \times Q_{\text{elec}}^{-1}(\mathbf{r_1}, T_{\text{elec}}) \ . \tag{23}$$

Note the above derivation is very similar to that of the configurational-bias MC (CBMC) scheme [28–32]. The only difference is that the last term in Eqs. (22) and (23), which is a summation in the original CBMC scheme (called Rosenbluth weight), is substituted here by an integration, Q_{elec} (for quadratic-coupling cases, however, Q_{elec} is just a constant independent of the nuclear coordinates). By definition, the superdetailed balance condition between these two states is

$$\begin{aligned} &P(\mathbf{r_1}, \mathbf{q_1}) \times T_{\mathbf{r}_2}(\mathbf{q_2}) \times \text{acc}(\Gamma_1 \to \Gamma_2) \\ &\quad = P(\mathbf{r_2}, \mathbf{q_2}) \times T_{\mathbf{r}_1}(\mathbf{q_1}) \times \text{acc}(\Gamma_2 \to \Gamma_1) \ . \end{aligned} \tag{24}$$

Substituting Eqs. (22) and (23) gives

$$\begin{aligned} &P(\mathbf{r_1}, \mathbf{q_1}) \times \exp\left(-\frac{\epsilon_2}{k_{\text{B}}T_{\text{elec}}}\right) \\ &\quad \times Q_{\text{elec}}^{-1}(\mathbf{r_2}, T_{\text{elec}}) \times \text{acc}(\Gamma_1 \to \Gamma_2) \\ &= P(\mathbf{r_2}, \mathbf{q_2}) \times \exp\left(-\frac{\epsilon_1}{k_{\text{B}}T_{\text{elec}}}\right) \\ &\quad \times Q_{\text{elec}}^{-1}(\mathbf{r_1}, T_{\text{elec}}) \times \text{acc}(\Gamma_2 \to \Gamma_1) \ . \end{aligned} \tag{25}$$

Reorganizing the Eq. (25) using $\text{acc}(\Gamma_1 \to \Gamma_2)/\text{acc}(\Gamma_2 \to \Gamma_1) = \exp[-(E_2 - E_1)/k_{\text{B}}T]$ (see Eq. 21) yields

$$\begin{aligned} &\exp\left(\frac{E_1}{k_{\text{B}}T}\right) \times \exp\left(\frac{\epsilon_1}{k_{\text{B}}T_{\text{elec}}}\right) \times Q_{\text{elec}}(\mathbf{r_1}, T_{\text{elec}}) \times P(\mathbf{r_1}, \mathbf{q_1}) \\ &\quad = \exp\left(\frac{E_2}{k_{\text{B}}T}\right) \times \exp\left(\frac{\epsilon_2}{k_{\text{B}}T_{\text{elec}}}\right) \\ &\quad \times Q_{\text{elec}}(\mathbf{r_2}, T_{\text{elec}}) \times P(\mathbf{r_2}, \mathbf{q_2}) \ . \end{aligned} \tag{26}$$

Since both sides are independent of each other,

$$\begin{aligned} &\exp\left(\frac{E_1}{k_{\text{B}}T}\right) \times \exp\left(\frac{\epsilon_1}{k_{\text{B}}T_{\text{elec}}}\right) \times Q_{\text{elec}}(\mathbf{r_1}, T_{\text{elec}}) \times P(\mathbf{r_1}, \mathbf{q_1}) \\ &\quad = \mathscr{A} \end{aligned} \tag{27a}$$

$$\begin{aligned} P(\mathbf{r_1}, \mathbf{q_1}) = &\exp\left(-\frac{E_1}{k_{\text{B}}T}\right) \times \exp\left(-\frac{\epsilon_1}{k_{\text{B}}T_{\text{elec}}}\right) \\ &\times Q_{\text{elec}}^{-1}(\mathbf{r_1}, T_{\text{elec}}) \times \mathscr{A} \ , \end{aligned} \tag{27b}$$

where $\mathscr{A}$ is a constant. Generalizing the above equation for any state, with coordinates $(\mathbf{r}, \mathbf{q})$, with the ground-state energy $E_{\text{gs}}(\mathbf{r})$, the electronic energy $\epsilon(\mathbf{r}, \mathbf{q})$, and the total energy $E(\mathbf{r}, \mathbf{q})$ $[= E_{\text{gs}}(\mathbf{r}) + \epsilon(\mathbf{r}, \mathbf{q})]$, we obtain

$$\begin{aligned} P(\mathbf{r}, \mathbf{q}) &= \exp\left(-\frac{E(\mathbf{r}, \mathbf{q})}{k_{\text{B}}T}\right) \times \exp\left(-\frac{\epsilon(\mathbf{r}, \mathbf{q})}{k_{\text{B}}T_{\text{elec}}}\right) \\ &\quad \times Q_{\text{elec}}^{-1}(\mathbf{r}, T_{\text{elec}}) \times \mathscr{A} \\ &= \exp\left(-\frac{E_{\text{gs}}(\mathbf{r})}{k_{\text{B}}T}\right) \times \exp\left(-\frac{\epsilon(\mathbf{r}, \mathbf{q})}{k_{\text{B}}T'_{\text{elec}}}\right) \\ &\quad \times Q_{\text{elec}}^{-1}(\mathbf{r}, T_{\text{elec}}) \times \mathscr{A} \end{aligned} \tag{28a}$$

$$\frac{1}{T'_{\text{elec}}} = \frac{1}{T_{\text{elec}}} + \frac{1}{T} \ . \tag{28b}$$

Integration of Eq. (28a) over all possible values of $\mathbf{q}$ gives

$$\begin{aligned} \int P(\mathbf{r}, \mathbf{q}) d\mathbf{q} = \mathscr{A} \int &\exp\left[-\frac{E_{\text{gs}}(\mathbf{r})}{k_{\text{B}}T}\right] \times \exp\left[-\frac{\epsilon(\mathbf{r}, \mathbf{q})}{k_{\text{B}}T'_{\text{elec}}}\right] \\ &\times Q_{\text{elec}}^{-1}(\mathbf{r}, T_{\text{elec}}) d\mathbf{q} \end{aligned} \tag{29a}$$

$$P(\mathbf{r}) = \mathscr{A}' \times \exp\left[-\frac{E_{\rm gs}(\mathbf{r})}{k_{\rm B}T}\right] \times Q_{\rm elec}(\mathbf{r}, T'_{\rm elec}) \times Q^{-1}_{\rm elec}(\mathbf{r}, T_{\rm elec}) \ . \tag{29b}$$

After normalization one obtains

$$P(\mathbf{r}) = \frac{\exp\left[-\frac{E_{\rm gs}(\mathbf{r})}{k_{\rm B}T}\right] \times Q_{\rm elec}(\mathbf{r}, T'_{\rm elec}) \times Q^{-1}_{\rm elec}(\mathbf{r}, T_{\rm elec})}{\int \exp\left[-\frac{E_{\rm gs}(\mathbf{r})}{k_{\rm B}T}\right] \times Q_{\rm elec}(\mathbf{r}, T'_{\rm elec}) \times Q^{-1}_{\rm elec}(\mathbf{r}, T_{\rm elec}) d\mathbf{r}} \ . \tag{30}$$

As already demonstrated, for quadratic-coupling cases, $Q_{\rm elec}(\mathbf{r}, T_{\rm elec})$ is independent of the nuclear coordinates. Thus, the electronic partition functions cancel, $P(\mathbf{r})$ becomes equal to $\rho(\mathbf{r})$, and sampling of the nuclear degrees of freedom from the BO limit [see Eq. (20b)] is achieved. In this case, the canonical partition function of the combined system can be separated into the nuclear part and the electronic part:

$$Q_{\rm ne} = Q_{\rm nucl}(T) \times Q_{\rm elec}(T'_{\rm elec}) \tag{31a}$$

$$Q_{\rm nucl}(T) = \mathscr{C} \int \exp\left[-\frac{E(\mathbf{r})}{k_{\rm B}T}\right] d\mathbf{r} \tag{31b}$$

$$Q_{\rm elec}(T'_{\rm elec}) = \mathscr{C}' \int \exp\left[-\frac{\epsilon(\mathbf{s})}{k_{\rm B}T'_{\rm elec}}\right] d\mathbf{s} \tag{31c}$$

$$P(\mathbf{s}) = \exp\left[-\frac{\epsilon(\mathbf{s})}{k_{\rm B}T'_{\rm elec}}\right] \Big/ \int \exp\left[-\frac{\epsilon(\mathbf{s})}{k_{\rm B}T'_{\rm elec}}\right] d\mathbf{s} \ . \tag{31d}$$

In Eq. (31d), the **s** coordinates denote the normal electronic coordinates after the linear transformation which are independent of the **r** coordinates. Therefore, the probability of visiting a certain nuclear configuration is consistent with the BO limit independent of $T_{\rm elec}$. The ensemble average of the total energy should be

$$\langle E_{\rm total} \rangle = \langle E_{\rm BO} \rangle + 0.5 N_{\rm elec} k_{\rm B} T'_{\rm elec} \ . \tag{32}$$

The above theoretical results agree with those given by the numerical tests on the *xy* and *AaBb* model problems, and the SPC-FQ water-dimer and bulk-water systems. For most cases reported above, $T_{\rm elec} \ll T$, so $T'_{\rm elec} \simeq T_{\rm elec}$ (see eq. 28b). The offset of the average total energy compared to the BO value is close to $0.5 N_{\rm elec} k_{\rm B} T_{\rm elec}$; however, for the water-dimer system at $T_{\rm elec} = 50$ K, the electronic contribution to the total dimer energy was observed to be 87 K (the energy divided by $k_{\rm B}$), which is much lower than $0.5 N_{\rm elec} T_{\rm elec} = 100$ K, but is in good agreement with $0.5 N_{\rm elec} T'_{\rm elec} = 86$ K. The RDFs, which represent the probability distributions of the nuclear coordinates, are consistent with those using the MM-MC method for all $T_{\rm elec}$.

Some additional tests on the *xy* problem and the water-dimer systems were carried out to investigate the above theoretical results at higher $T_{\rm elec}$. For the *xy* problem, $d_x = d_y = 1$ and $R_{\rm elec} = 100$ were used. $T_{\rm elec}$ was chosen from the following values, 0.1, 1, 5, and 50. The distributions of the *x* coordinate are compared to the analytical solutions for the BO limit in Fig. 16. It is evident that the choice of $T_{\rm elec}$ does not affect the *x* (nuclear) coordinate distribution. Even at $T_{\rm elec} \gg T$, the probability distribution of the *x* coordinate still reproduced the BO limit. In addition, the probability distributions of the $s\,(=y-x)$ coordinate (Fig. 16) were found to satisfy the following equation:

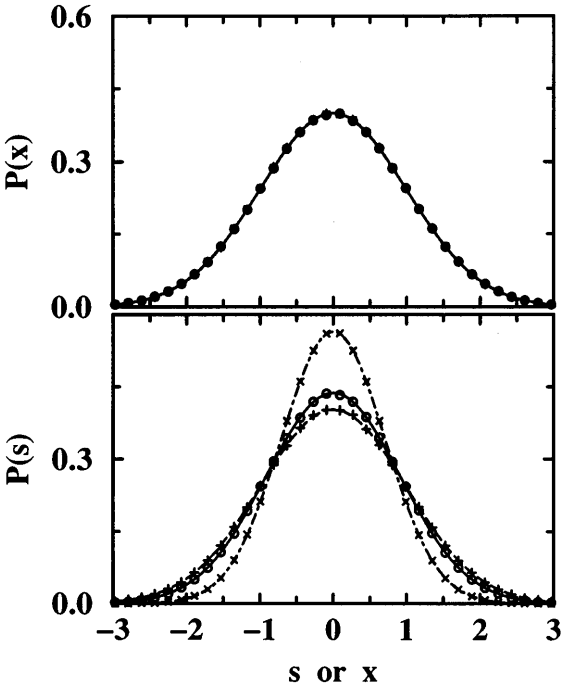

Fig. 16. Probability distribution of the *x* (*top*) and *s* (*bottom*) coordinate for the *xy* problem using the ANES-MC algorithm with $d_x = d_y = 1$ and $R_{\rm elec} = 100$. *Crosses*, *circles*, and *plusses* denote results for $T_{\rm elec} = 1$, 5, and 50, respectively. The BO limit probability distribution of the *x* coordinate is shown as the *solid line*. Probability distributions of the *s* coordinate calculated from Eq. (33) for $T_{\rm elec} = 1$, 5, and 50, are shown as *dashed-dotted*, *solid* and *long dashed lines*

$$P(s) = \frac{1}{\sqrt{2T'_{\rm elec}\pi}} \exp\left(-\frac{s^2}{2T'_{\rm elec}}\right) \ . \tag{33}$$

This is consistent with Eq. (31d). The average energies for $T_{\rm elec} = 1$, 5, and 50, are 0.750, 0.916, and 0.989, respectively, while the theoretical results calculated from Eq. (32) are 0.750, 0.917, and 0.990. For the water dimer, some additional tests were carried out at $T_{\rm elec} = 150$, 300 and 600 K. Plots of $\langle E_{\rm dimer} \rangle$ versus $T'_{\rm elec}$ show linear behavior, while plots of $\langle E_{\rm dimer} \rangle$ versus $T_{\rm elec}$ clearly show curvatures at high $T_{\rm elec}$ (Fig. 7). A linear fit of $\langle E_{\rm dimer} \rangle$ versus $T'_{\rm elec}$ (for $R_{\rm elec} = 1000$) yields a slope of 2.0 and an intercept of −458 K, i.e. excellent agreement with the theoretical results calculated from Eq. (32). These additional tests using higher $T_{\rm elec}$ further support our theoretical arguments above.

Similar observations were found in molecular dynamics simulations. Sprik [18] used the adiabatic extended Lagrangian technique to investigate the influence of the electronic temperature on the simulation results on his polarizable water model, in which the electronic degrees of freedoms are coupled in a quadratic form. Changing the electronic temperature from 5 to 300 K did not alter the liquid-water structure. In calculations of the

heat of vaporization, Sprik added $0.5N_{\rm elec}k_{\rm B}T_{\rm elec}$, which was attributed to the thermal disorder, and found that the heat of vaporization was lower at $T_{\rm elec} = 300$ K.[1] Sprik argued that the polarization fluctuations are correlated and that the correlation energy is negative. Sprik also pointed out that unlike the static averages and the vibrational frequencies, the diffusion constants and other relaxation rates are extremely sensitive to the choice of $T_{\rm elec}$, and that thermal polarization fluctuations as well as delayed responses of the polarization dynamics inhibit diffusion. The amount of $0.5N_{\rm elec}k_{\rm B}T_{\rm elec}$, attributed to the thermal disorder, may be corrected to $0.5N_{\rm elec}k_{\rm B}T'_{\rm elec}$ because the electronic degrees of freedom are coupled with the nuclear degrees of freedom, and thus the polarization fluctuations are correlated (this has been demonstrated by us for the water dimer using a high $T_{\rm elec}$).

In the ANES-MC algorithm, the partition function defined in Eq. (31a) is only correctly sampled under the following conditions:

1. The electronic configurations of both initial and trial nuclear configurations are within the skin thickness of the BO surface.
2. The electronic configuration is sampled from its correct distribution, otherwise, the superdetailed balance condition shown in Eq. (24) is violated

To satisfy these two conditions, a small step size in the nuclear move or a large number of electronic moves are required. For the SFQ-MC algorithm, Eq. (24) is only approximately satisfied using a small step size and a small $T_{\rm elec}$.

One important point is that for all the systems reported in Sect. 3, the electronic degrees of freedom are coupled in a quadratic form. The quadratic coupling ensures that the degeneracies of the electronic levels, $\omega(\epsilon)$, and thus also the electronic phase-space volume, $Q_{\rm elec}$, are identical for every nuclear configuration; however, this is not true for all kinds of coupling between electronic and nuclear degrees of freedom. In cases where the coupling is not quadratic, $Q_{\rm elec}(\mathbf{r}, T_{\rm elec})$ may be dependent on the nuclear coordinates. It is evident from Eq. (30) that $P(\mathbf{r})$ is no longer proportional to $\exp[-E_{\rm gs}(\mathbf{r})/k_{\rm B}T]$ unless $T_{\rm elec} \to 0$ when $T'_{\rm elec} \simeq T_{\rm elec}$ and $Q_{\rm elec}(\mathbf{r}, T'_{\rm elec})/Q_{\rm elec}(\mathbf{r}, T_{\rm elec})$ is approaching unity. Starting from the xy model, we investigated two examples of nonquadratic coupling

$$E' = \frac{1}{2}\left(x - y^3\right)^2 + \frac{1}{2}x^2 \quad \text{and} \quad E'' = \frac{1}{2}\left(x - y^{1/3}\right)^2 + \frac{1}{2}x^2 \ . \tag{34}$$

In the BO limit, the probability distributions for the x coordinates remain the same as for the original xy problem with quadratic coupling (see Eq. 5a).

The ANES-MC algorithm was applied to the above two cases using $T = 1$ and $R_{\rm elec} = 1000$. The maximum nuclear displacements were $d_x = d_y = 0.1$. Two different $T_{\rm elec}$ were chosen: 0.01 and 0.1. The distributions of x are plotted in Fig. 17 and compared to those obtained for the original problem. At $T_{\rm elec} = 0.01$, the distributions of x are indistinguishable and agree with the BO limit. At $T_{\rm elec} = 0.1$, however, coupling 1 (y^3) obviously favors the low-energy state. In contrast, for coupling 2 ($y^{1/3}$), x coordinates close to zero are less often sampled; however, the distribution for the original xy problem remains close to the BO limit for $T_{\rm elec} = 0.1$. This is strong evidence that the ANES-MC algorithm is only rigorously valid for problems where the electronic degrees of freedom are coupled in a quadratic form or where the probability distributions of the electronic energy levels, $P(\epsilon)$, is identical for every nuclear configuration. For the systems with y^3 and $y^{1/3}$ coupling, the probability distributions of the electronic energy levels are dependent on the nuclear coordinates (Fig. 18). For $y^{1/3}$ coupling, from Eq. (29),

$$P(x) = \exp\left(-\frac{x^2}{2}\right) \times \left(\frac{x^2}{T'_{\rm elec}} + 1\right) \times \left(\frac{x^2}{T_{\rm elec}} + 1\right)^{-1} \times \mathscr{A} \ . \tag{35}$$

From Eq. (35), the most probable state can be determined. For $T_{\rm elec} = 0.1$, $x \simeq \pm 0.2$ is the most probable state, which is consistent with the numerical tests (Fig. 17). Integration of Eq. (35) gives the correct partition function for a finite $T_{\rm elec}$.

Finally, we would like to discuss the issue of coordinate transformations. Linear transformations work only when the highest-order term is linear or quadratic and they conserve the total phase-space volume because only rotations and translations are used to

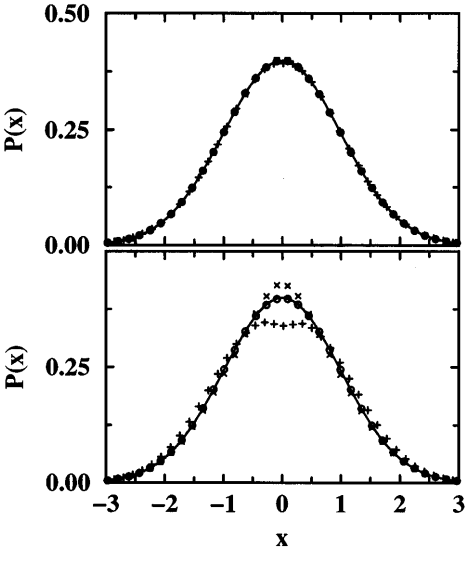

Fig. 17. Probability distributions of the x coordinate for the xy problem with three different couplings calculated with the ANES-MC algorithm ($d_x = d_y = 0.1$, $R_{\rm elec} = 1000$, and $T = 1$): $V = \frac{1}{2}(x-y)^2 + \frac{1}{2}x^2$ (*circles*), $V' = \frac{1}{2}\left(x - y^3\right)^2 + \frac{1}{2}x^2$ (*crosses*), and $V'' = \frac{1}{2}\left(x - y^{1/3}\right)^2 + \frac{1}{2}x^2$ (*plusses*). *Top* and *bottom* panels show results for $T_{\rm elec} = 0.01$, and 0.1, respectively

[1] It should be pointed out that the electronic degrees of freedom will contribute to the same extent to the average energy of molecules in the vapor phase. Thus, heats of vaporization calculated from Gibbs ensemble simulations will not be affected by the offset in energy stemming from the electronic degrees of freedom.

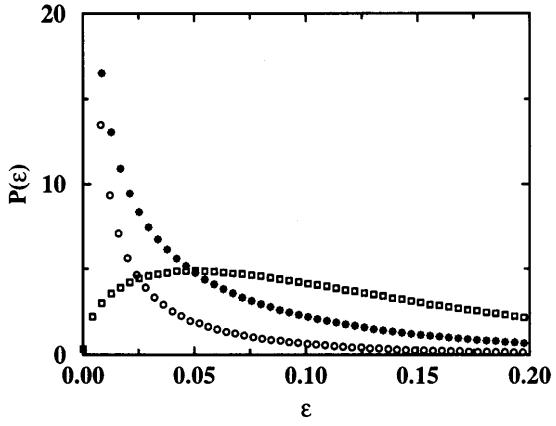

Fig. 18. Probability distributions of the electronic energy levels for the *xy* problem: $V' = \frac{1}{2}(x - y^3)^2 + \frac{1}{2}x^2$ at $x = 0$ (*circles*) and $x = 1$ (*crosses*), and $V'' = \frac{1}{2}(x - y^{1/3})^2 + \frac{1}{2}x^2$ at $x = 0$ (*squares*) and $x = 1$ (*diamonds*)

obtain the new coordinate space. With the help of the linear transformation, the coupled degrees of freedom in the old coordinate space can be decoupled in the new space. In this sense, it can be used to separate the nuclear and transformed electronic degrees of freedom and to perform the adiabatic sampling. This can be easily demonstrated for the *xy* problem. When the normal coordinate $s = x - y$ is introduced, sampling of the x and s coordinates involves two uncoupled harmonic oscillators with two different temperatures and the adiabatic limit is automatically satisfied; however, for more complicated systems such as bulk SPC-FQ water, finding the normal coordinates for the electronic degrees of freedom (or the corresponding linear transformation) is even more difficult than locating the ground-state configuration. Thus it is not a practicable approach to separate the electronic degrees of freedom.

8 Conclusions

Three different MC techniques (SFQ-MC, ANES-MC, and MM-MC) for adiabatic sampling of nuclear and electronic degrees of freedom were applied to four model systems, ranging from simple coupled harmonic oscillators to bulk SPC-FQ water. While the SFQ-MC and ANES-MC algorithms require only trivial changes to any existing MC program, the MM-MC algorithm is more difficult to program. The MM-MC method always samples from the limiting BO distribution, but is, in practice, too computationally expensive for large systems, because its computing-time requirement scales as N^4 per MC cycle. Conventional iterative MC schemes for polarizable force fields scale as N^3. In contrast, the computing-time requirements for SFQ-MC and ANES-MC increase only as N^2 under certain conditions (e.g. small nuclear displacements and preferential sampling). The SFQ-MC algorithm proposed in our previous communication [21] was designed to mimic the Car–Parrinello method in a MC framework. Since nuclear and electronic moves are performed sequentially in the SFQ-MC algorithm, it will only yield the correct ensemble distributions if the maximum displacements for nuclear moves are sufficiently small to ensure that nuclear moves do not depart from the skin thickness of the BO surface. This problem severely limits the applicability of the SFQ-MC algorithm and will prevent its use for simulations in the grand-canonical and Gibbs ensembles. The ANES-MC algorithm, however, overcomes this problem by introducing a physically more appealing way to deal with electronic fluctuations: the electronic states are sampled "on-the-fly" during a nuclear move. It has been demonstrated that in the limit of $R_{\text{elec}} \to \infty$ and $T_{\text{elec}} \to 0$, the ANES-MC method becomes equivalent to the MM-MC method. The same holds true for the SFQ-MC algorithm, but with the extra condition that the nuclear step sizes approach zero.

ANES-MC simulations for bulk liquid water ($N = 100$) have demonstrated that limiting the maximum nuclear displacements allows one to use relatively few electronic moves, thereby greatly improving the computational efficiency. The reason for this is that small nuclear displacements allow the system to remain within the skin thickness of the BO surface. Monitoring the energy evolution during the electronic move sequence in ANES-MC is a helpful tool to find a good set of simulation parameters (nuclear and electronic displacements and number of electronic moves). In general, reducing the electronic temperature will increase the computational burden. Straightforward extensions allow one to perform ANES-MC simulations in the isobaric–isothermal, grand-canonical and Gibbs ensembles.

In addition to the numerical tests, a canonical partition function has been presented for systems containing nuclear and electronic degrees of freedom with adiabatic separation. The canonical partition function can be separated into a nuclear part and an electronic part independent of T_{elec} under a quadratic coupling of the electronic degrees of freedom. For nonquadratic coupling cases, satisfactory sampling of the nuclear coordinate phase-space requires a low T_{elec} to limit the ratio of the phase-space volumes of the electronic degrees of freedom at two different temperatures, T_{elec} and T'_{elec}, to be close to unity.

Acknowledgements. We would like to thank Glenn Martyna, Mark Tuckerman, and Woods Halley for many stimulating discussions. Financial support from the National Science Foundation (grant NSF CTS-9813601), the Petroleum Research Fund, administered by the American Chemical Society, a Camille and Henry Dreyfus New Faculty Award, a McKnight/Land-Grant Fellowship, an Alfred P. Sloan Research Fellowship, and a Stanwood Johnston Memorial Fellowship (B.C.) is gratefully acknowledged. Part of the computer resources were provided by the Minnesota Supercomputing Institute.

References

1. Allen MP, Tildesley DJ (1987) Computer simulation of liquids. Oxford University Press, Oxford
2. Frenkel D, Smit B (1996) Understanding molecular simulation. Academic Press, San Diego

3. Sprik M, Klein ML (1988) J Chem Phys 89: 7556
4. Ahlström P, Wallqvist A, Engström S, Jönsson B (1989) Mol Phys 68: 563
5. Cieplak P, Kollman P, Lybrand T (1992) J Chem Phys 97: 13841
6. Rick SW, Stuart SJ, Berne BJ (1994) J Chem Phys 101: 6141
7. Wallqvist A, Berne BJ (1993) J Phys Chem 97: 13841
8. Chialvo AA, Cummings PT (1996) J Chem Phys 105: 8274
9. Svishchev IM, Kusalick PG, Wang J, Boyd RJ (1996) J Chem Phys 105: 4742
10. Car R, Parrinello M (1985) Phys Rev Lett 55: 2471
11. Anderson HC (1980) J Chem Phys 72: 2384
12. Saboungi ML, Rahman A, Halley JW, Blander M (1988) J Chem Phys 88: 5818
13. Wilson M, Madden PA (1993) J Phys Condens Matter 5: 2687
14. Gao J, Pavelites JJ, Habibollazadeh D (1996) J Phys Chem 100: 2689
15. Medeiros M, Costas ME (1997) J Chem Phys 107: 2012
16. Kiyohara K, Gubbins KE, Panagiotopoulos AZ (1998) Mol Phys 94: 803
17. Remler DK, Madden PA (1990) Mol Phys 70: 921
18. Sprik M (1991) J Phys Chem 95: 2283
19. Pastore G, Smargiassi E, Buda F (1991) Phys Rev A 44: 6334
20. Galli G, Pasquarello A (1992) In: Allen MP, Tildesley DJ (eds) Computer simulation in chemical physics. NATO ASI Series. Kluwer, Dordrecht, pp 261
21. Martin MG, Chen B, Siepmann JI (1998) J Chem Phys 108: 3383
22. Berendsen HJC, Postma JPM, van Gunsteren WF, Hermans J (1981) In: Pullman B (ed) Intermolecular forces: Proceedings of the 14th Jerusalem Symposium on Quantum Chemistry and Biochemistry. Kluwer, Dordrecht, pp 331
23. Martyna GJ, Tuckerman M, Klein ML (1992) J Chem Phys 97: 2635
24. Nosé S (1984) Mol Phys 52: 255
25. Hoover WG (1985) Phys Rev A 31: 1695
26. Soper AK, Turner J (1993) Int J Mod Phys B 7: 3049
27. Pangali C, Rao M, Berne BJ (1978) Chem Phys Lett 55: 413
28. Siepmann JI (1990) Mol Phys 70: 1145
29. Siepmann JI, Frenkel D (1992) Mol Phys 75: 59
30. Frenkel D, Mooij GCAM, Smit B (1992) J Phys Condens Matter 4: 3053
31. de Pablo JJ, Laso M, Suter UW (1992) J Chem Phys 96:2395
32. Siepmann JI (1993) In: van Gunsteren WF, Weiner PK, Wilkinson AJ (eds) Computer simulation of biomolecular systems: theoretical and experimental applications, vol 2. ESCOM Science, Leiden, p 249